The Palette of Fronts and Cyclones within a Baroclinic Wave Development

H. C. DAVIES, CH. SCHÄR* AND H. WERNLI

Atmospheric Physics, ETH Zürich, Switzerland

(Manuscript received 26 June 1990, in final form 8 February 1991)

ABSTRACT

A study is undertaken of the concurrent development of fronts and cyclones within a growing baroclinic wave. The dynamical framework for the study is that of the semigeostrophic, adiabatic flow of a uniform potential vorticity atmosphere that is sandwiched between two horizontal plates on an f plane. A three-dimensional spectral model is used to examine the growth to finite amplitude of the normal modes of this system for basic states that comprise of a symmetric jetlike baroclinic flow with (and without) a superposition of a uniform barotropic shear of either cyclonic or anticyclonic vorticity. It is demonstrated that the presence of such lateral shear in the ambient environment exerts a profound influence upon the ensuing palette of fronts and cyclones.

On the synoptic scale this flow component influences the scale and strength of the individual surface highs and lows, and also modifies the extent of their lateral drift away from, and their relative movement along, the baroclinic zone. Aloft, the development of the trough–ridge system is altered appreciably with positive (negative) shear favoring the formation of cutoff cold (warm) air pools. On the subsynoptic scale the lateral shear induces a selective frontogenetic effect; e.g., positive shear sustains surface warm fronts and suppresses surface cold frontogenesis. The range of simulated frontal phenomena includes frontal fracture, warm air seclusion and a bent-back warm front. In particular for a weak ambient positive barotropic shear the evolving frontal palette acquires the distinctive and characteristic λ-shaped configuration.

Theoretical considerations and diagnostic analyses provide insight upon the sensitivity of the flow response to the lateral shear. At root it is shown to be related to two intrinsic symmetry features of the semigeostrophic system. In the quasi-linear phase of the development the shear induces a displacement of the critical-surface of the wave relative to the main baroclinic zone, a concomitant asymmetric modification in the structure of the normal modes, and a substantial positive feedback upon the shear of the mean flow. The latter changes effectively determine the lateral and relative movement of the pressure systems as well as their spatial scale. The diagnostic analyses also serve to pinpoint, for the nonlinear phase of the development, the salient single level and upper level–lower level interactions that drain and reverse the zonal-mean surface baroclinicity in midstream, force the perturbations to overshoot the baroclinic zone, and engender the rich subsynoptic scale features.

Consideration is given to the relationship with observed weather systems and to the physical and mathematical limitations of the simulations.

1. Introduction

Cold and warm fronts are invariably depicted on surface synoptic charts as integral ingredients of two types of patterns. They are either shown as the main component of an incipient cyclone wave growing within a frontal zone or, in combination with their occluded progeny, as the subsynoptic embroidery of a maturing or mature low pressure system. There is nevertheless often some uncertainty in the prescription of the frontal palette to be associated with individual cyclogenesis events. For example, the classic process of occlusion comprising a cold front overtaking a warm front is probably a rare feature of cyclogenesis (Palmen 1951; Wallace and Hobbs 1977). Again warm fronts do not necessarily feature as a part of the palette, and their demarcation often merely signifies the existence of an amorphous band of "weather" in the vicinity. Likewise there is a wide variation in the spatial scale, intensity, and the relative-geometric configuration of the cyclones and anticyclones that accompany the frontogenesis events. The structure of, and the linkage between, these pressure systems and fronts form the underlying theme of the present study.

Our current understanding of contemporaneous cyclo- and frontogenesis derives principally from the inductive synthesis of observational data and deductive studies with research and forecast numerical models. Substantial reviews that encompass both of these categories can be found in Newton and Holopainen (1990). Here we restrict our introductory remarks to issues that pertain to the present study.

The early observational studies concentrated primarily on surface data and led to the association of surface cold and warm frontal zones with certain salient

* *Current Affiliation:* Department of Geology and Geophysics, Yale University, New Haven, Connecticut.

Corresponding author address: H. C. Davies, Atmospheric Physics, ETH, Hönggerberg, CH-8093 Zürich, Switzerland.

flow characteristics (an enhanced horizontal thermal gradient, a wind shift and convergence of the horizontal velocity field, significant prefrontal bands of strong relative airflow), and to the surface frontal-wave theory of cyclogenesis. Inductive studies in this vein have subsequently sought to extend the concept of prefrontal airstreams into a full three-dimensional picture (e.g., see Browning 1990), and recast the frontal wave model in the framework of balanced flow dynamics (Shapiro 1983). Recent case-study analyses of comparatively small-scale, combined cyclo- and frontogenesis events (Shapiro and Keyser 1990) utilizing a data base of unusually fine spatial resolution revealed several distinctive features along with the cold and warm frontogenesis. These included a fracture of the original baroclinic zone such that the cold front is dislocated from the cyclone, the occurrence of a clearly defined seclusion, and the presence of a strong bent-back warm front arching from the cyclone rear across its inner northern core before extending eastwards.

Other of the early inductive-type studies centered on the relationship between upper-level structures and surface cyclogenesis. Subsequent consolidation and extension of this work on the vertical coupling is documented by Reed (1990). In particular Kleinschmidt (1950) and more recently Hoskins et al. (1985) provided cogent evidence of the influence of upper-level effects from the standpoint of potential vorticity dynamics. (A tacit quid pro quo inference is that the surface frontal palette might also be triggered or modulated by upper-level effects.)

Deductive studies, the second of the aforementioned categories, have examined the link between synoptic-scale flow and frontogenesis using both quasi two-dimensional and three-dimensional theoretical models. The former class of study is geared specifically to elucidating the nature of the frontogenesis that results from the presence, in certain idealized but germane flow configurations, of a vertical and/or horizontally aligned deformation flow component (e.g., see Keyser and Pecnick 1987, and the references therein). Studies with three-dimensional models have included the examination of frontal development within growing normal-mode baroclinic waves (e.g., Hoskins and West 1979; Hoskins 1983; Takayabu 1986; Polavarapu and Peltier 1990). Simulations with semigeostrophic models of baroclinic wave development within a uniform potential vorticity (PV) atmosphere (Hoskins and West 1979, hereafter referred to as HW) yielded credible cold frontal structures from jetlike basic states. However, the instigation of a warm front in the SE quadrant of the cyclone was achieved only by specifying a "relative" easterly jet structure for the ambient low-level state and at the expense of entirely suppressing the development of the cold front. Normal mode simulations undertaken with PE models develop a richer and contemporaneous mix of frontal structures. In this case the simulations can also be extended further into the nonlinear regime, and pronounced seclusions form as an advancing cold front merges with the trailing tail end of the cold front associated with the preceding cyclone. In view of these significant differences the utility of the semigeostrophic system as an appropriate *limit-form* of the PE system for the study of baroclinic wave development is currently a subject of discussion.

Again, high resolution limited-area NWP models also have the potential to, and do, predict on a day-to-day basis both cyclogenesis and the development and movement of the accompanying cold and warm fronts (Woodroffe 1984). Such models have also been used to hindcast certain observed rapid cyclogenesis events and to assess the relative importance of various adiabatic and diabatic processes (see the review of Uccellini 1990). The frontal features that evolve in such models bear comparison with the real development. For example, a simulation reported in Shapiro and Keyser (1990) of an observed event displayed successively a wave-development, frontal fracture, seclusion, and a bent-back warm front.

In the present study we follow the deductive approach and use, as in HW, an idealized semigeostrophic model of a uniform PV atmosphere. A study is made of the linear and the finite-amplitude features of unstable normal modes growing on baroclinic jetlike basic states. The aim is to reexamine the palette of fronts and cyclones that develops within such growing baroclinic waves.

The additional ingredient in our study, over and above that considered in HW, relates to the breaking of a symmetry feature of simple baroclinic systems. In the *present context* the most basic symmetry-breaking factor is the presence of a uniform ambient barotropic shear superimposed on the standard (e.g., HW) symmetric baroclinic jet. Aspects of the influence of barotropic shear upon baroclinic wave development have been considered in several earlier studies. The simulations of HW, although not violating the symmetry criterion, did reveal a strong sensitivity to low-level lateral shear. Again Simmons and Hoskins (1980) and James (1987) used a PE model cast in spherical geometry to consider the impact of barotropic shear upon the development. In keeping with the resolution of their model, they chose to examine the barotropic shear's modification of the gross, as opposed to the frontal, features. James demonstrated the subtle influence of this shear component upon the growth rate and the structure of the unstable normal modes. More recently Thorncroft and Hoskins (1990) used a PE model to examine the structures that develop within an unstable baroclinic wave in the finite-amplitude regime, and on this basis they argued that the in situ lateral shear exerts a strong influence upon the occurrence of upper level cutoff features.

Here we systematically appraise in the context of our model flow system the sensitivity of the baroclinic wave development to the inclusion of the uniform

barotropic shear. In particular we explore the influence of this shear upon the nature of the "front–cyclone" palette.

2. The dynamical framework

a. *Outline of the model and the method*

The system considered is that of the semigeostrophic flow of an adiabatic, inviscid, and incompressible fluid of uniform potential vorticity sandwiched between two horizontally aligned rigid surfaces located on an f plane.

In this limit a mathematical transformation renders the flow system isomorphic to the standard geostrophic set (Hoskins 1975). The transformation is defined by

$$X = x + v_g/f; \quad Y = y - u_g/f; \quad Z = z; \quad T = t; \tag{2.1}$$

where (x, y, z, t) and (X, Y, Z, T) represent, respectively, Cartesian coordinates in physical and geostrophic space, and (u_g, v_g) are the geostrophic flow components. It is thus mathematically convenient and physically insightful to consider the flow dynamics in geostrophic space. Application of the inverse of the transform (2.1) enables the flow fields to be viewed in physical space. (Note that the model system adopted follows that of HW except that our z coordinate corresponds to physical height as opposed to their pseudoheight. The two systems are essentially isomorphic.)

The system of equations in the transformed space are nondimensionalized in accord with Table 1. It then follows that the stipulation of a uniform PV atmosphere leads to a harmonic equation for the geostrophic streamfunction (ψ) in the interior; i.e.,

$$\psi_{XX} + \psi_{YY} + \psi_{ZZ} = 0, \tag{2.2}$$

while at the surface and the upper rigid lid the advection equation for the potential temperature takes the form:

$$\frac{\partial \theta}{\partial T} + u_g \frac{\partial \theta}{\partial X} + v_g \frac{\partial \theta}{\partial Y} = 0 \quad \text{at} \quad Z = (0, Z_T) \tag{2.3a}$$

where

$$\theta = \frac{\partial \psi}{\partial Z}.$$

TABLE 1. Setting for the nondimensional variables.

Horizontal length scale	a	2000 km
Vertical length scale	af/N	20 km
Horizontal velocity scale	U	48 m s^{-1}
Rossby number	U/af	0.24
Time scale	a/U	11.6 h
Temperature scale	$UN\Theta/g$	14 K
Pressure scale	$aUf\rho_0(z)$	96 hPa at $z = 0$ 70 hPa at $z = 9$ km

This simple mathematical specification [i.e., Eqs. (2.2)–(2.3)] constitutes the reduced form that the so-called invertibility principle (Hoskins et al. 1985) takes for this flow system: *the dynamics of the uniform PV atmosphere is determined entirely by the spatial distribution and development of the potential temperature on the surface and the lid.*

To investigate the nature of the "front–cyclone" palette we adopt a two-step approach. First, a linear normal mode stability analysis is undertaken of certain (see next subsection) basic states, $V = V(X, Z)$ and $\vartheta = \vartheta(X, Z)$, that in physical space possess flow and thermal fields reminiscent of the temporal and zonal mean conditions of the midlatitude troposphere. Here we have followed the usual convention in theoretical frontal studies and orientated the Y axis along the baroclinic zone with the X axis pointing toward the warm air. Also for convenience we will refer, respectively, to the (X, Y) axes as the meridional and pseudozonal directions (with X taken to point southward). For this linear problem the prognostic equation for the surface and upper-lid potential temperature reduces to the form:

$$\left(\frac{\partial}{\partial T} + V\frac{\partial}{\partial Y}\right)(\theta') + u'\frac{\partial \vartheta}{\partial X} = 0 \quad \text{at} \quad Z = (0, Z_T) \tag{2.3b}$$

where the prime variables denote the deviation away from the basic state (V, ϑ). The stability analysis is undertaken in conjunction with the long term numerical integration of the linearized system—a technique that yields only the fastest growing mode for each prescribed zonal (i.e., Y-orientated) wavelength.

In the second step the development of the most unstable normal modes of each prescribed basic state is followed into the finite-amplitude regime until the semigeostrophic transformation (2.1) breaks down. To perform the associated numerical integration we proceed as follows:

- the geostrophic streamfunction is split into the two harmonic components of a basic state, $\Psi(X, Z)$, and the deviation therefrom;
- the boundary conditions in the zonal direction are provided by the periodicity of the normal mode;
- the condition adopted at the lateral boundaries corresponds to periodic continuation (i.e., periodicity is assumed only for the deviation component of the flow field in the direction perpendicular to the basic flow);
- the width of the computational domain is chosen to extend over approximately four dimensionless units. For physical credence, the amplitude of the deviation component should be very small near the lateral boundaries (this is verified a posteriori);
- the potential temperature field at the surface and upper rigid lid of the model domain is represented by 64×64 spectral components.

Further details of the model and the numerical procedures can be found in Schär and Davies (1990).

b. The basic state

The basic state geostrophic streamfunction, $\Psi(X, Z)$, is assigned the following three-component form,

$$\Psi(X, Z) = -\frac{1}{2}\left[\arctan\frac{X}{1+Z} - \arctan\frac{X}{1-Z}\right] + 0.12XZ + \frac{1}{2}A(X^2 - Z^2). \quad (2.4)$$

These components constitute, respectively, a ramplike baroclinic zone, a uniform baroclinic field, and a uniform barotropic shear coupled to a uniform stratification. (Hereafter, flow profiles with and without the third component will be usually referred to, respectively, as the sheared and unsheared cases.)

In Fig. 1 the cross-sectional structure of the basic state in physical space is displayed for the unsheared ($A = 0$) case and for one particular sheared case ($A = +0.1$). The flow specification yields an enhanced baroclinic zone of width ~2000 km, and surface temperature contrast of ~15 K. (This thermal transition zone is significantly more laterally confined than the configuration adopted in HW, although both are characterized by the same thermal wind speed maximum.) For the unsheared case (Fig. 1a) the accompanying thermal wind is zero at the ground, forms an upper-level jet of U_{max} (~30 m s^{-1}), and the associated vorticity maxima (not shown) are $\pm 0.3f$. Note that the transformation of (2.4) induces a weak asymmetry of the flow pattern in physical space; e.g., the jet axis is shifted a distance (U_{max}/f) ~300 km north of mid-channel. For the sheared case (Fig. 1b) there are only minor modifications with a uniform decrease of the potential temperature at the lid by 0.6 K and an enhancement of the relative vorticity of the entire domain by $0.024f$. The additional shear corresponds to a wind of ±4.8 m s^{-1} at a lateral distance of ±2000 km with an associated pressure difference of 4.8 hPa over the same distance.

c. Two mathematical symmetries

There are, *for the problem as posed above,* two significant symmetries associated with our flow system.

1) SYMMETRY A

This symmetry pertains in geostrophic space. It applies to the linear and the finite-amplitude phase of the development of pairs of normal modes of the basic state (2.4) that are characterized by equal but opposite values of the shear parameter A. For the ψ field it implies that the paired fields are mirrored in the sense that

$$\psi_+(X, Y, Z, T) = -\psi_-(-X, Y, Z, T) \quad (2.5)$$

where $\psi_{+(-)}$ denotes the streamfunction in the case of an ambient cyclonic ($A > 0$) and anticyclonic ($A < 0$) shear.

This result follows from noting that both the basic state (2.4) and the associated normal mode fulfill the condition (2.5), and that applying the transformation

$$\langle A \to (-A); X \to (-X) \rangle,$$

changes the signs of each term in both Eqs. (2.3a) and (2.3b). Thus if the condition (2.5) is fulfilled initially, it will remain valid in the subsequent linear and nonlinear phase of the development.

It follows that consideration of the influence of shear upon the nature of the solutions in geostrophic space can be limited to, say, the cyclonic shear case [the fields for the anticyclonic case can be inferred from Eq. (2.5)]. One implication is that the dispersion relationship for the normal modes does not depend on the sign

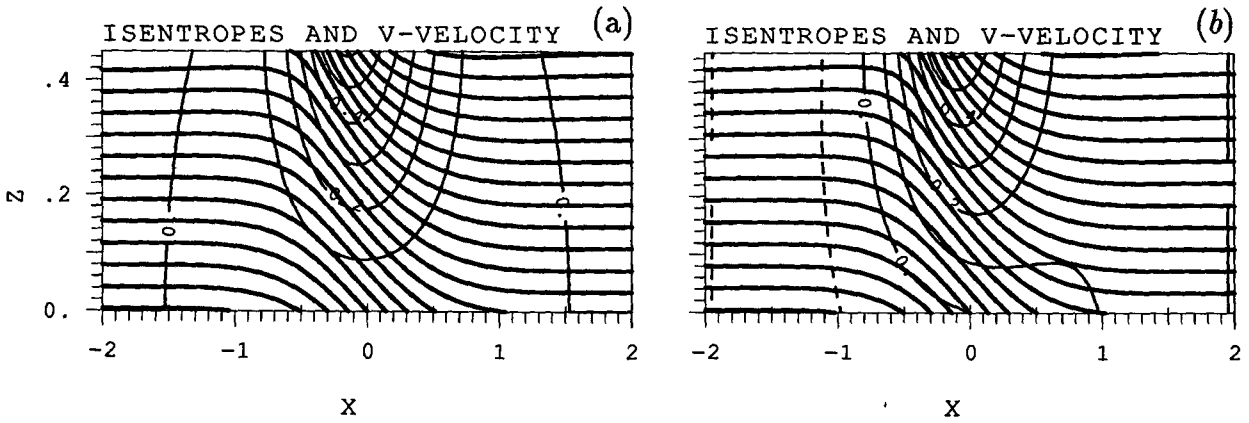

FIG. 1. Vertical sections across the specific baroclinic zone in physical space (a) for the unsheared case, $A = 0$, and (b) for the case of cyclonic shear, $A = +0.1$. The bold lines are isentropes with an isoline spacing of 0.2 (~2.8 K); the thin lines mark the zonal wind speed with an isoline spacing of 0.1 (~4.8 m s^{-1}). The depicted domain covers (8000 × 9) km.

of the shear parameter; i.e., both the growth rate and phase speed of the normal modes are the same for equal and opposite values of A. These latter features were already noted by James (1987).

2) SYMMETRY B

This symmetry is more fundamental to our study and pertains to the flow structure in geostrophic space for the case of $A = 0$. It is evident in the pattern of the surface temperature and pressure fields in both geostrophic and physical space. Figure 2 shows these fields at a particular time in the nonlinear development of the most unstable normal mode of the pure baroclinic jet (this case will be discussed in some detail later). In the figure, "twin" thermal bands located astride the baroclinic zone have been opaqued to highlight the feature under consideration.

The symmetry takes the form

$$\psi(X, Y, Z, T) = -\psi(-X, Y - \lambda/2, Z, T), \quad (2.6)$$

where λ denotes the wavelength of the feature. Similar relations hold for the potential temperature and relative vorticity. Likewise the geostrophic flow components satisfy the equations,

$$u_g(X, Y, Z, T) = -u_g(-X, Y - \lambda/2, Z, T), \quad (2.7a)$$

$$v_g(X, Y, Z, T) = +v_g(-X, Y - \lambda/2, Z, T). \quad (2.7b)$$

The basis for a theorem embodying this symmetry property is outlined in the Appendix. In the form given there the symmetry holds only in transformed space. However, there is one specific feature that also pertains in physical space: at the center of low and high pressure systems the geostrophic wind vanishes, and hence at these locations the transformation (2.1) reduces to the identity $(x, y) = (X, Y)$. Thus the east–west separation (i.e., distance along the Y axis) of consecutive high and low pressure centers remains constant.

It follows that a severe geometric constraint is placed upon both linear and nonlinear structures of the semi-geostrophic normal modes of a symmetric baroclinic zone. The symmetry can be broken in various ways, e.g., by adding a purely asymmetric component to the basic state itself, by introducing a β effect, or by internal PV gradients. To explore the consequences of breaking the symmetry it is appropriate to introduce the most dynamically inert modification of the basic state. The addition of a uniform horizontal shear flow component with the form of the third term in Eq. (2.4) meets this stipulation—from the standpoint of so-called "potential vorticity dynamics" it contributes only an additional small uniform temperature increment at the lid and induces no change in the internal PV.

3. Features of the linear instability

a. The spectra

The stabilty analysis of baroclinic basic states is a recurring theme in dynamical meteorology, and there have been numerous recent studies of the stability of baroclinic jetlike flows (e.g., Simmons and Hoskins 1976, 1980; Ioannu and Lindzen 1986; James 1987; Moore and Peltier 1989; Valdes and Hoskins 1988). Here, such an analysis is a prerequisite for our study of the nonlinear phase of the development, and it permits us to ascertain a posteriori to what extent the structure of the normal modes provides a key to the understanding of the resulting cyclone and frontal palette.

Spectra are shown in Fig. 3 for the growth rate, $\sigma = \sigma(l)$, and the phase speed, $c_r = c_r(l)$, derived for different values of the ambient shear of the baroclinic basic state. For the $A = 0$ case the most unstable mode has a wavelength of ~3600 km, an e-folding time of ~2 days, and a phase speed approximately one-third

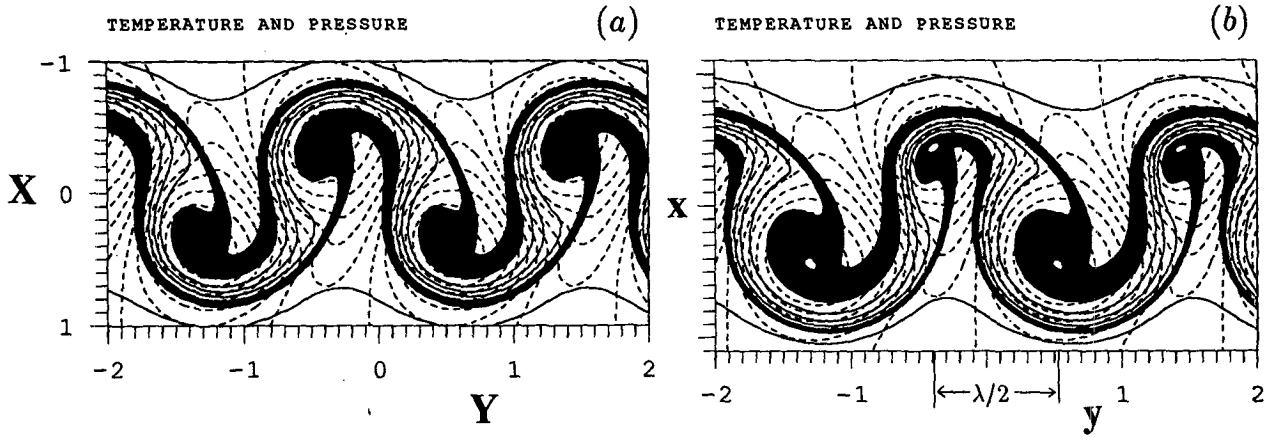

FIG. 2. A portrayal of symmetry B for the nonlinear normal-mode development in (a) geostrophic and (b) physical space. The solid lines are isentropes and the dashed lines isobars. "Twin" thermal bands located astride the baroclinic zone are opaque and the white spots within these bands mark the centers of the pressure systems.

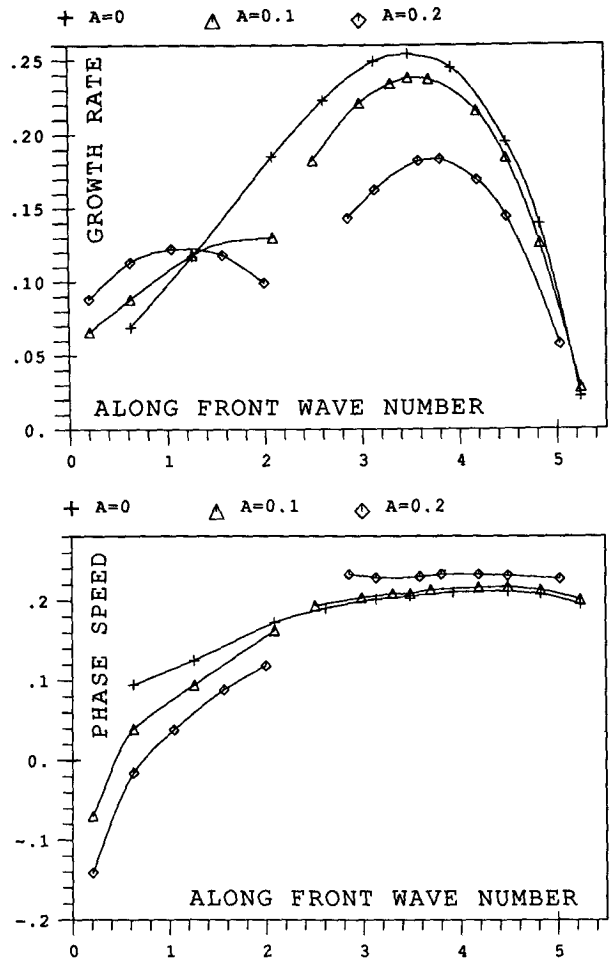

FIG. 3. Growth rate and phase speed spectra displayed as a function of the "zonal" wavenumber (l) for different values of the shear parameter A. The dimensionless scales are such that $c_r = 0.1$ corresponds to 4.8 m s^{-1}; whilst $\sigma = 0.1$ corresponds to 2.4×10^{-6} s^{-1} or 0.21 day^{-1} and likewise $l = 1$ scales to 5×10^{-7} m^{-1}.

that of the wind speed maximum in the jet. Introduction of a lateral shear induces a noticeable reduction in the growth rate (cf. James 1987) but only a mild increase in the phase speed and wavelength of the most unstable mode. (The secondary long wavelength mode that is favored at larger absolute values of A is a result of an instability associated with a thermal extremum on a bounding surface (cf. Schär and Davies 1990), and for such long wavelengths the vertical depth scale of these modes is proportional to the width of the extremum. A minimal adjustment of the basic state to remove the feature eliminates these particular modes without significantly modifying the pseudo-Eady modes).

b. *The structure of the modes*

Figure 4 shows, for the unsheared case ($A = 0$), the normal mode structure *in transformed space* of the perturbation fields of potential temperature, pressure, and relative vorticity. For reference purposes, note that for a thermal perturbation maximum at the surface of unit value (~14 K) the accompanying pressure and vorticity maxima at that level are, respectively, 0.2 (~19.2 hPa) and $4.4R_0$ ($\sim 1.1f$), while the thermal, pressure and vorticity signals at the lid take the respective values of 1.1 (~15.4 K), 0.24 (~16.8 hPa.) and $5.6R_0$ ($\sim 1.4f$). In agreement with previous studies (see in particular HW) the perturbation fields tilt horizontally with the jet throughout the depth to form "swept-back" wing structures. The amplitudes on the two bounding surfaces are comparable, and the upper-level thermal pattern leads that at the surface by slightly less than a quarter of a wavelength. At the upper level the fields, particularly the relative vorticity, show a stronger lateral phase change. Note that in physical space the centers of the upper-level patterns are aligned along the jet axis and are thus located north of the channel center.

Figure 5 is the analogue of the previous figure for the case of an ambient positive ($A = 0.1$) barotropic shear. The presence of the shear increases the amplitude and the tilt of the northern wing while there is a decrease in the length scale characterizing its lateral scale. In contrast the tilt of the southern wing is reduced while it retains its lateral length scale. Also indicated in the upper panels of Figs. 4 and 5 is the location, if present in the displayed domain, of the critical lines. The latitudinal shift (~200 km southward for $A = 0.1$) in the location of the critical lines is a significant fraction of the width of the baroclinic zone.

Recall that for the case of negative shear the normal mode structure can be obtained by invoking the property associated with symmetry A.

c. *Interpretation and implications*

1) THE GROSS FEATURES

Instabilities of quasi-geostrophic/balanced flows can be usefully interpeted in terms of the interaction of two "Rossby" wave trains (Hoskins et al. 1985). For the present flow configuration the two wave trains are essentially boundary-trapped baroclinic waves propagating, respectively, on the surface and the upper lid of the flow domain, and the waves are confined principally to the region of enhanced baroclinicity on those two boundaries. In the absence of an interaction between the two wave trains, the lower and upper waves would possess respectively an eastward and westward directed propagation velocity relative to the flow at their level. However the "upper level–lower level" wave interaction will modify this counterpropagation, and for a suitable phasing of the two wave trains they can remain stationary relative to one another and also experience synchronous growth.

Phenomenologically based semiquantitative arguments can be advanced to support this conceptual in-

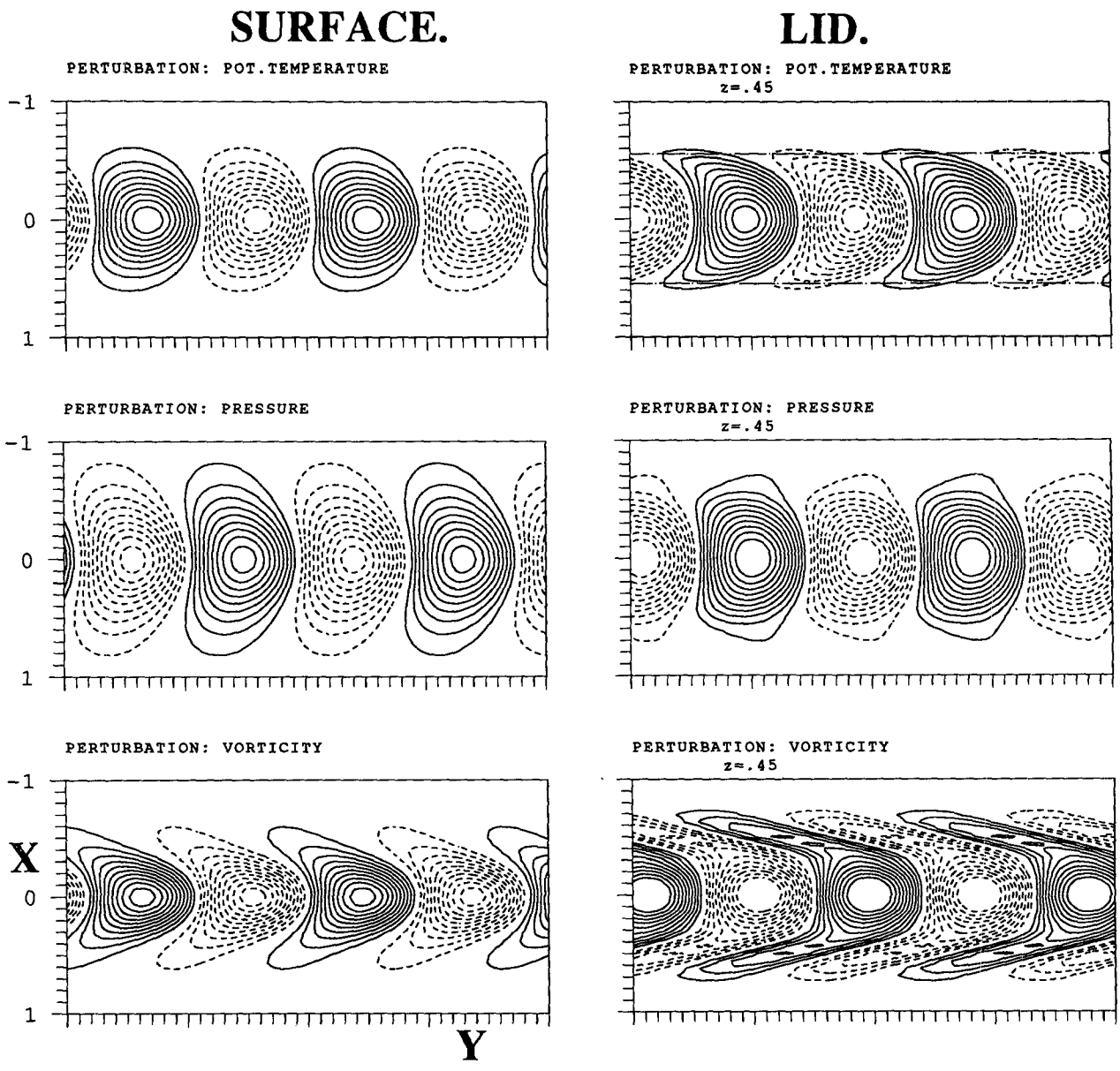

FIG. 4. The normal-mode structure in geostrophic space for the unsheared case ($A = 0$). Displayed are the perturbation fields of potential temperature, pressure and relative vorticity at the surface (panels on the left) and at the rigid lid (panels on the right). Negative contours are dashed and the dot-dashed lines in the panels for the potential temperature indicate the locations of the critical line. (See text for an indication of the relative values of the three flow variables.)

terpretation. These arguments also pertain in the presence of a *weak* uniform barotropic shear, and hence suggest that for such a configuration there will only be minor modification of the gross spatial features, growth rate, and phase speed of the normal modes.

2) THE FINE-SCALE STRUCTURE

To aid in the interpretation of the finer scale features evident on the bounding surfaces, we write the geostrophic streamfunction and potential temperature of the normal mode in the general form,

$$\psi' = \tilde{\Psi} \exp i[l(Y - cT) + \gamma]$$

$$\partial\psi'/\partial Z = \tilde{\Theta} \exp i[l(Y - cT) + \gamma + \epsilon]$$

where the amplitudes $(\tilde{\Psi}, \tilde{\Theta})$ and phases $(\gamma, \gamma + \epsilon)$ are functions of both X and Z, and the complex phase speed, $c = (c_r, c_i)$, is such that $\sigma = l \times c_i$.

It can then be deduced from Eq. (2.3b) that, at the bounding surfaces, the parameter-pair (κ, ϵ), signifying, respectively, the ratio of the amplitudes and the relative phase of ψ' and ψ'_Z are given by

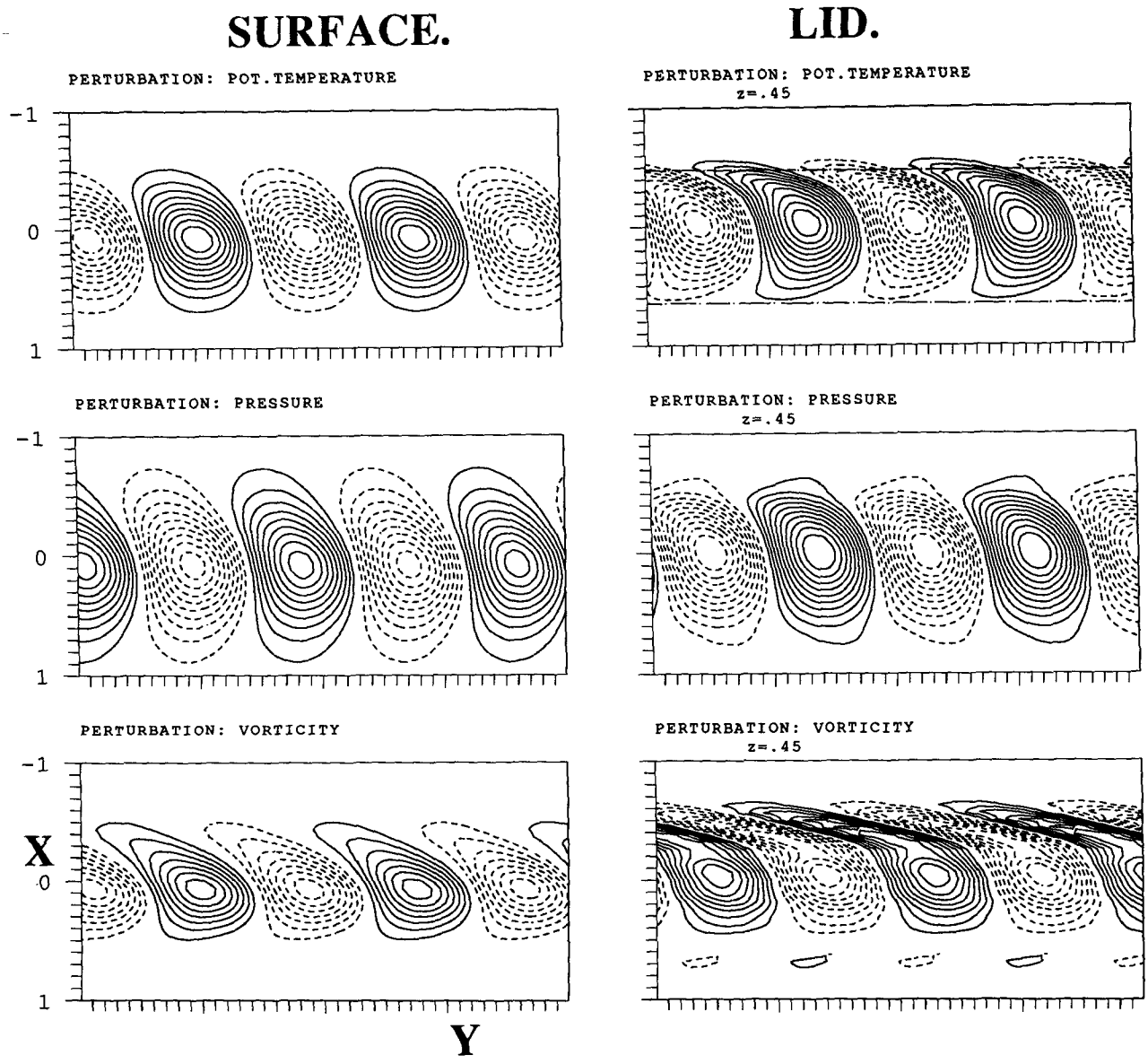

FIG. 5. As for Fig. 4, but for the cyclonic shear case ($A = +0.1$).

$$\kappa = \frac{\tilde{\Theta}}{\tilde{\Psi}} = \frac{\partial V/\partial z}{\mathcal{V}}, \tag{3.7}$$

$$\tan\epsilon = \frac{c_i}{(V - c_r)}, \tag{3.8}$$

and

$$\frac{\partial \gamma}{\partial z} = \frac{c_i \partial V/\partial z}{\mathcal{V}^2}, \tag{3.9}$$

where

$$\mathcal{V}^2 = [(V - c_r)^2 + c_i^2].$$

In the limit of γ being a weak function of z and $|\tan\epsilon| \ll 1$, then κ is the local measure of the decay rate of the mode away from the bounding surface and it is also a measure [see (2.2)] of the inverse of the local meridional length scale of the perturbation. Hence in this limit the variation of κ is an indicator of the change in the horizontal phase tilt of the perturbation. In addition, note that the vertical phase variation of γ is related to the meridional heat flux since

$$(\overline{u'\theta'}) \propto l|\psi|^2\left(\frac{\partial \gamma}{\partial z}\right).$$

Now consider the properties of the perturbations at the upper boundary. In midchannel the value of V and

(c_r, c_i) render $|\tan\epsilon| \ll 1$ and hence ψ' and ψ'_Z are almost in phase. In the adjacent regions the nature of the perturbations depends crucially upon the relative lateral decay rate of $(V - c_r)$ and $\partial V/\partial Z$. Two major classes can be distinguished for the perturbation structure.

Type (i): The critical line is located within the baroclinic zone [i.e., $(V - c_r) \to 0$ faster than $\partial V/\partial Z \to 0$], so that laterally κ increases, the vertical depth and the lateral scale decrease substantially, and the pattern tilts in toward midstream. At the critical line itself the thermal perturbation amplitude *can* sustain an appreciable amplitude but it is 90° out of phase with the pressure.

Type (ii): The critical line lies outside the main baroclinic zone (i.e., the decay rate of $\partial V/\partial Z$ dominates) and hence κ decreases, the depth and lateral scale of the perturbation increase and the pattern can maintain a meridional alignment.

For the case of the symmetric jet ($A = 0$) the first category prevails on both flanks of the jet and this accounts for the swept-back wings and the small lateral scale (Fig. 4). For the asymmetric cases the presence of, say, a positive barotropic shear induces the previously noted southward shift of the critical lines relative to the baroclinic zone. This results in a type (i) structure north of the jet and type (ii) to the south. It follows that in this case the perturbation fields are asymmetric with respect to midstream and tilt with the barotropic shear to the north of the jet maximum (Fig. 5).

At the ground the basic-state flow field is such that either there is no critical line (symmetric case) or it is in the far field (antisymmetric case). Hence a type (ii) structure prevails for both cases, and the phase difference ϵ is uniformly small. However, for the asymmetric case there will nevertheless be a small quantitative difference in the phase tilt on either side of the jet maximum. A further intriguing inference is that the northern critical line at the lid demarks, on the surface beneath it, a domain where the thermal perturbation will not be significant (cf. Fig. 5).

d. *The mean state tendencies and structural changes*

The influence of the normal modes upon the mean state can be inferred (cf. the invertibility principle for this system) from the temporal development of the zonal mean potential temperature, $\bar{\theta} = \bar{\theta}(X, Z, T)$, on the horizontal bounding surfaces. At these levels this tendency is given by the equation,

$$\frac{\partial \bar{\theta}}{\partial T} = -\frac{\partial(\overline{u'\theta'})}{\partial X}$$

where the overbar denotes the zonal average. To qualitatively relate this tendency to that of the zonal mean flow on the bounding surfaces recall that at the lower surface a local zonal mean warming (cooling) connotes a cyclonic (anticyclonic) modification of the zonal mean flow, while the reverse applies at the lid.

Figure 6 shows the meridional structure of the heat flux and heat flux-divergence on the bounding surfaces for the cases $A = 0$ and $A = 0.1$. In the unsheared case (Fig. 6a) the northward directed heat fluxes attain their extrema in midstream and are largest at the surface. The basic state baroclinicity is significantly smaller at this level and the larger value of the flux is achieved via the greater phase tilt ($\partial\gamma/\partial z$) of the perturbations. At the surface the flux divergence is such as to induce a westerly jet in midstream with attendant wings of easterly flow. On the other hand, at the lid the tendency is such as to reduce the strength of the existing jet in midstream and to build up the westerly flow on the wings. (Note that the horizontal phase tilts of the ψ' field itself implies an eddy momentum flux into the jet, and the inference is that this is overcome by a contribution of the mean meridional component of the ageostrophic perturbation.)

For the positive shear case (Fig. 6b) the amplitudes of the northward heat fluxes are comparable to those of the $A = 0$ case but the extremum at the surface (lid) is displaced slightly southward (northward). The accompanying change in the profile of flux-divergence at the lid induces diffuse and weak cooling to the south and a sharper and stronger warming to the north. It follows that the associated zonal flow tendencies will replicate those of the $A = 0$ case but with a shift to the south resulting in a concomitant enhancement of the ambient lateral shear in midstream.

The spatial form of the normal modes also provides some indication of possible structural changes that could occur to the thermal anomalies in the nonlinear phase of the development. An example is the vortex–vortex interaction of the thermal perturbations in midstream with those on the wings (in the linear limit this interaction is second order).

4. Description of the nonlinear development

Here the development into the nonlinear regime of the most unstable normal modes of the basic state is described for the case of no ambient barotropic shear ($A = 0$) and the cases with cyclonic and anticyclonic shear corresponding to $A = \pm 0.1$. The development is traced until the geostrophic transformation [i.e., Eq. (2.1)] breaks down and this occurs at around $t \approx 9$–10.

a. *The barotropically unsheared case*

Figure 7 shows the pressure and temperature distributions on the surface and the lid at various stages ($t = 6, 8, 10$) of the development. A depiction of the corresponding vorticity distributions at $t = 8$ is given in Figs. 10a,d. Also shown in Fig. 11a is one measure of the ageostrophic flow—the surface distribution of

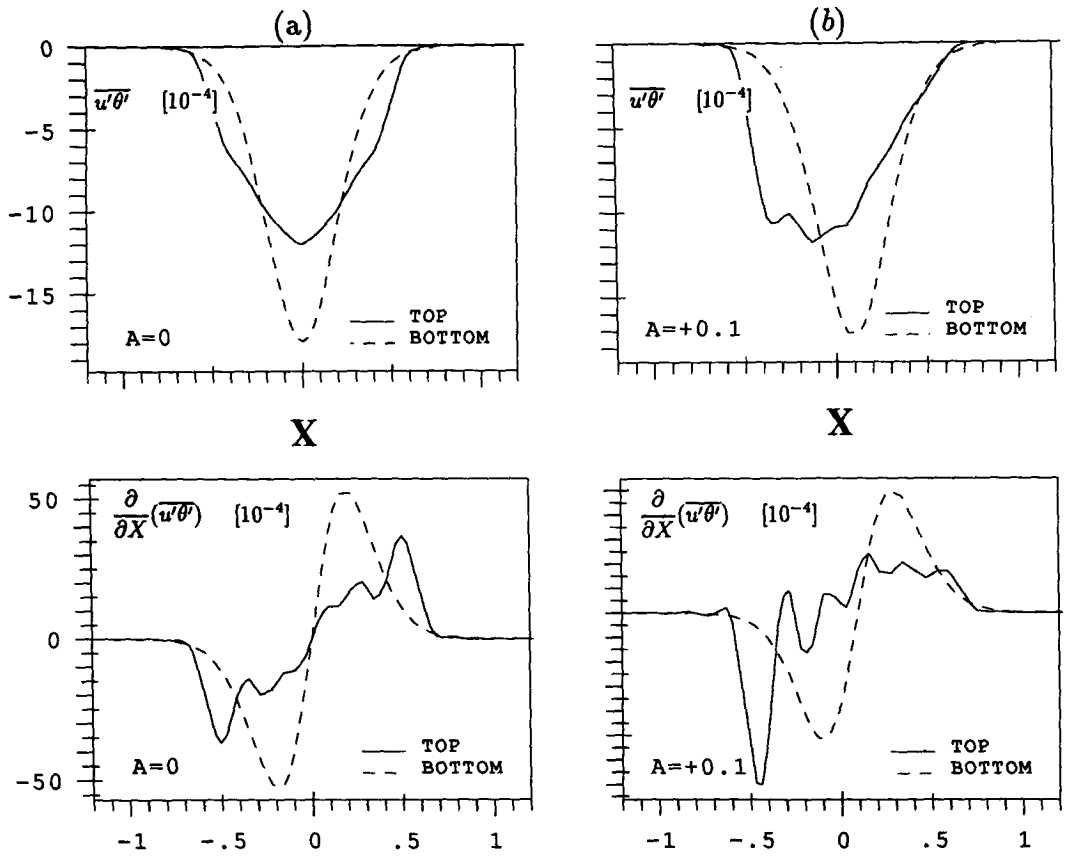

FIG. 6. Meridional structure of the heat flux and heat flux divergence on the bounding surfaces displayed in geostrophic space for (a) the unsheared case ($A = 0$) and (b) the cyclonic shear case ($A = +0.1$). The dimensionless (and dimensional) scales are based upon a thermal perturbation maximum of 0.175 K at the surface, and are given by 10^{-4} ($\sim$0.067 K m s^{-1}) for the heat flux and 10^{-4} ($\sim 3.4 \times 10^{-8}$ K s^{-1} = 0.003 K day^{-1}) for the heat flux divergence. A unit distance in X corresponds as usual to 2000 km.

the forcing function ($\mathcal{F}$ = div**Q**), of the quasi-geostrophic ω-equation (Hoskins et al. 1978). Here $\mathcal{F}$ has been calculated in geostrophic space but is displayed in physical space, and positive and negative values of $\mathcal{F}$ connote, respectively, surface divergence and convergence.

At the surface the incipient lows and highs drift, respectively, toward the northern and southern fringes of the original baroclinic zone. The surface cyclogenesis is accompanied by an extended northward incursion of a narrow tongue of warm air that curves cyclonically in toward the depression center forming an incipient seclusion. A broader band of cold air sweeps southward behind the cyclone and feeds the attendant anticyclogenesis. In this case all the structural differences between the low and the high are attributable to supra-geostrophic effects (i.e., they arise from the transformation back to real space). To the south of the surface cyclone the presence of distinct thermal gradient, wind shift and vorticity signatures are indicative of strong cold frontogenesis. The thermal gradient of the cold frontal band is rather weak in the vicinity of the cyclone itself, but to the southwest it extends around the base of the anticyclone. There is some evidence (see in particular Figs. 10a and 11a) of a weak, "stubby" warm front that extends directly outward and eastward from the cyclone center.

At the lid there is a southward encroachment of a cold air tongue. It induces cyclonic vorticity and is bordered on both its forward and rear flank by strong frontal features. On the forward edge of the accompanying trough this cold air curves cyclonically whereas it undergoes anticyclonic distortion on the rear southern side. The latter feature is linked to the broad northward protrusion of warm air and the anticyclonic vorticity of the associated ridge. The relative movement of the upper and lower features during the development is such that there is a decrease in the westward tilt with height of the pressure systems.

The general development bears a strong qualitative resemblance to the semigeostrophic simulations of HW (particularly their $\mu = 1.0$ case) although there are some quantitative differences of detail related to the adoption of a sharper basic state profile in the present study.

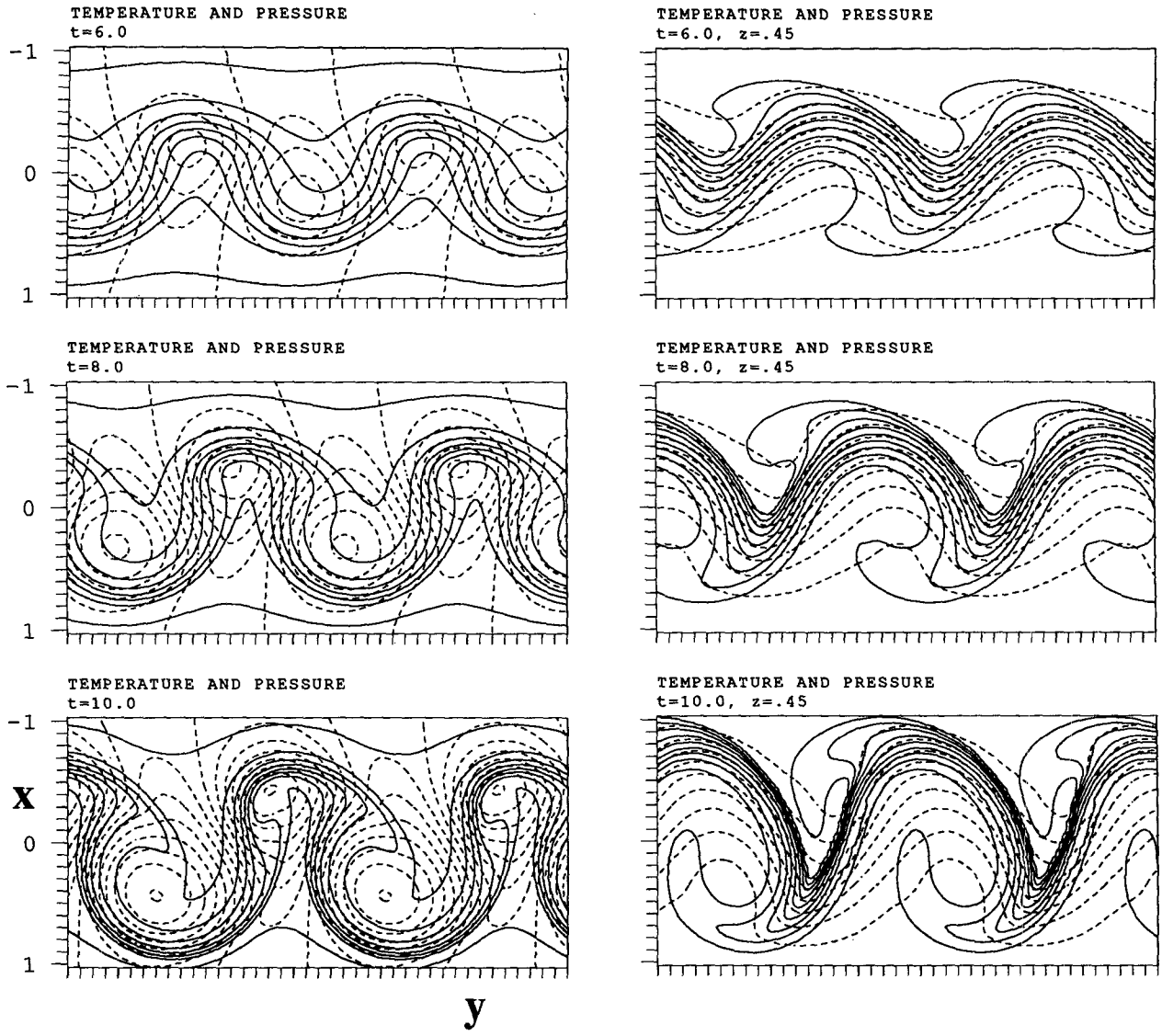

FIG. 7. The nonlinear normal-mode development for the unsheared case ($A = 0$) at the times $t = 6$, 8 and 10 (~day 3, 4 and 5) at both the surface (on the left) and the tropopause (on the right). The fields are displayed in physical space and the isoline spacings are 0.15 (~2 K) for the isentropes (solid lines), and 0.03 (~3 hPa) for the pressure (dashed lines) at the surface and 0.06 (~4.2 hPa) for the "tropopause" pattern.

b. The anticyclonic-shear case

In this case (see Fig. 8) the entire pattern of high–low development at the surface is shifted appreciably northwards. In comparison with the previous case the northeastward drifting surface lows evolve with a smaller spatial scale and advance zonally upon the preceding broader scale highs. The surface warm tongue now aligns itself almost linearly SW–NE (i.e., with the barotropic shear) and it ends in a secluded dumbbell to the SE of the surface low. The vorticity and $\mathcal{F}$-fields of the system at $t = 8$ (see Figs. 10b and 11b) indicate that the link between the cyclone and the cold front is now much stronger. There is little evidence of a separate warm-frontal feature.

At the lid there is a southward shift of the patterns, and it is the pressure ridge that advances upon the preceding trough. The southern extremity of the cold air is again bordered by frontal features, but in comparison with the previous case it undergoes less cyclonic deformation to the northeast and enhanced anticyclonic deformation to the southwest. The resulting vorticity pattern (see Fig. 11e) has a distinctive "Y" signature. The NE–SW stem of this signature is aligned parallel to the surface cold front so that this front has a measure of coherence throughout the depth. In stark contrast

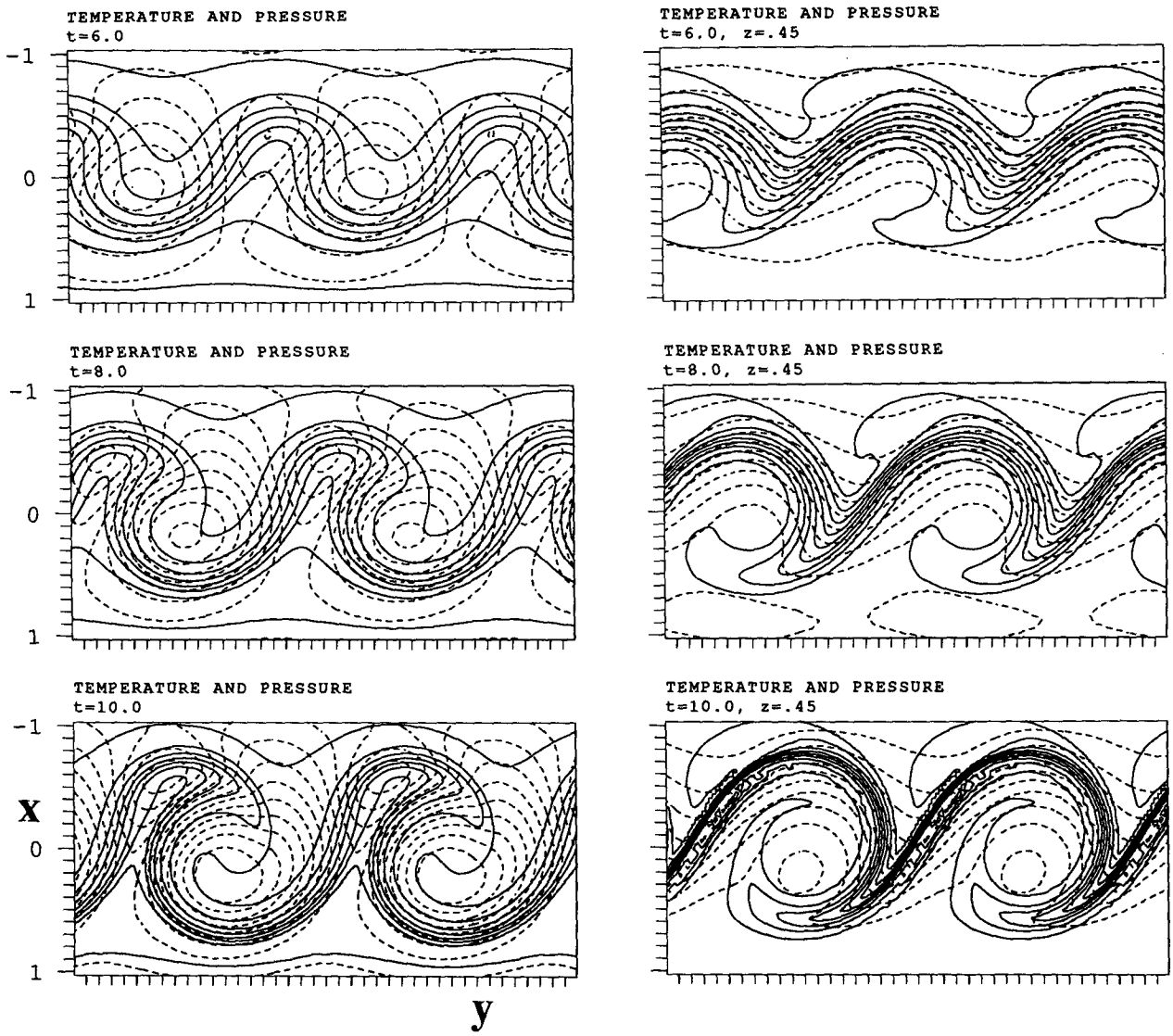

FIG. 8. As in Fig. 7 but for the case of anticyclone shear ($A = -0.1$).

to the unsheared case the westward tilt with height of the cyclones (anticyclones) increases (decreases) substantially during the development.

c. *The cyclonic-shear case*

In this case (see Fig. 9) the surface high–low pattern is displaced southward, and it is the relatively southerly located highs that advance zonally toward the more northerly located lows. This results in the generation of appreciably stronger winds to the SW of the surface depression. The surface warm tongue acquires a NW–SE orientation (i.e., again that of the basic-state barotropic shear), and it secludes cyclonically into the core of the low pressure system. To the southeast of the cyclone center, the thermal pattern of the cold front is severely disrupted (cf. the phenomenon of frontal fracture), while to the northwest and north there is evidence of a bent-back frontal feature that extends southeastward as a warm front. The frontal palette evident in the surface $\mathcal{F}$ field (Fig. 11c) develops a distinctive λ-shaped configuration reminiscent of the cloud pattern associated with many observed systems.

At the lid the anticyclonic distortion of the cold trough, evident south of the jet in the $A = (0, -0.1)$ cases, is virtually absent. Now this protrusion secludes on the forward flank of the upper-level trough. The accompanying vorticity pattern (Fig. 10f) assumes a "stem plus barrel" configuration. The barrel links with the surface low to establish a coherent quasi-vertical cyclonic system. Likewise the stem that extends out toward the northwest is aligned parallel to and ahead of the surface warm front of the succeeding surface low.

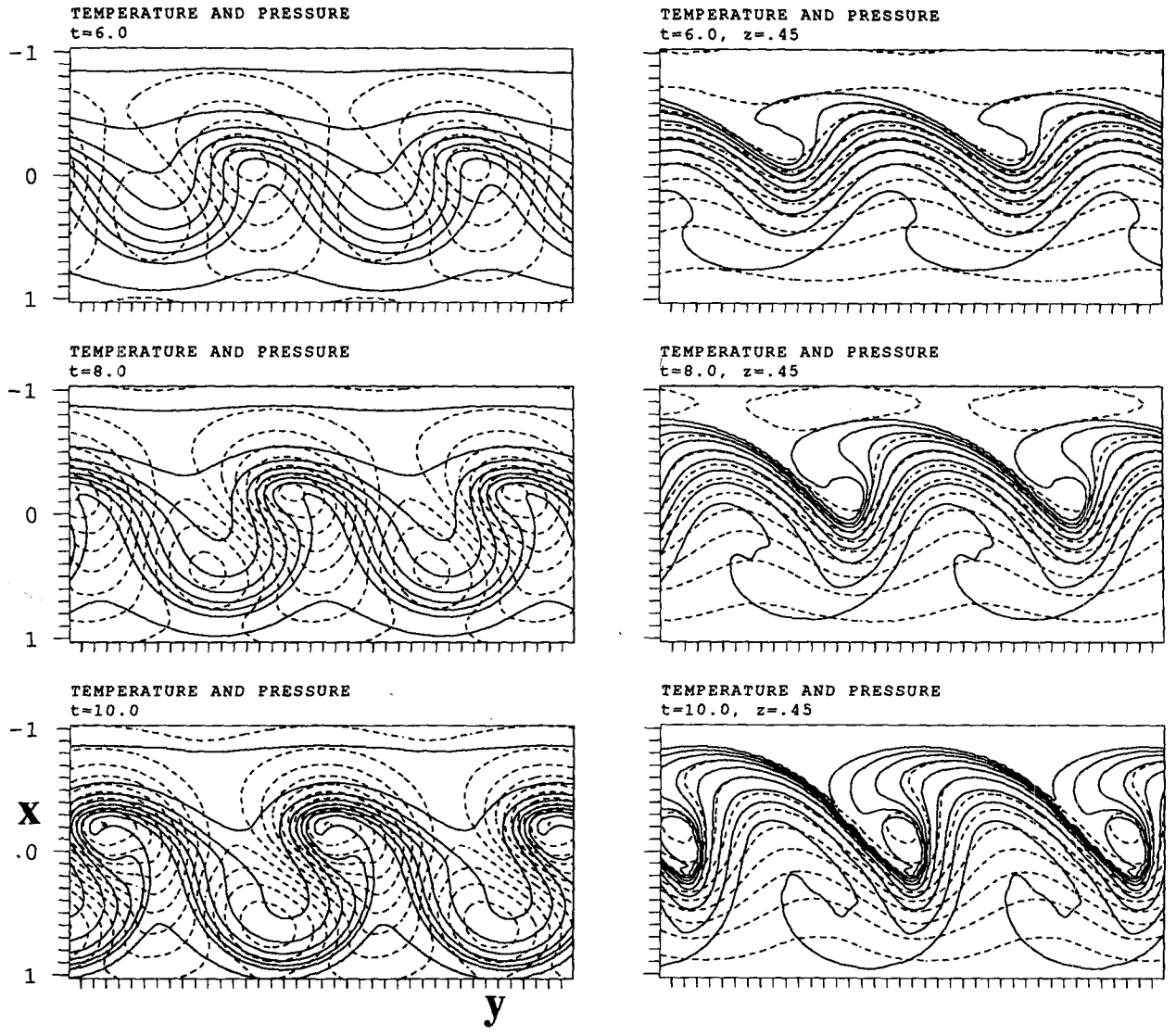

FIG. 9. As in Fig. 7 but for the case of cyclonic shear ($A = +0.1$).

5. Diagnosis of the nonlinear development

It is again appropriate to interpret the flow features in terms of the evolution of the thermal patterns on the two bounding surfaces. From a PV standpoint the impact of these patterns is mediated by the flow that they "engender" on the bounding surfaces. Furthermore, the flow on one boundary can be attributed to the sum of two components:

- the contribution linked to the thermal field at the given level, and
- the far-field contribution of the thermal pattern on the other bounding surface.

It also proves helpful to partition the potential temperature (θ) on these surfaces into zonal-mean ($\bar{\theta}$) and deviation (θ') components.

a. The two-phased development

Inspection of the θ' field development in geostrophic space, (see Fig. 12 for the $A = 0$ case and Fig. 13 for the $A = 0.1$ case) along with the accompanying $\bar{\theta}$ distribution (Fig. 14) reveals a two-phased development. There is an initial quasi-linear phase during which the perturbations grow and translate in substantial accord with the properties of the pertinent normal mode, and the changes to the zonal mean baroclinicity are as anticipated earlier (see Fig. 6 and the accompanying discussion). Thus, in contrast with the lateral drift northward and southward, respectively, of the surface lows and highs, the maximum amplitude of the perturbation anomaly patterns remain essentially in midstream. Also in this phase the zonal-mean baroclinicity within the central zone decreases in amplitude but remains almost uniform.

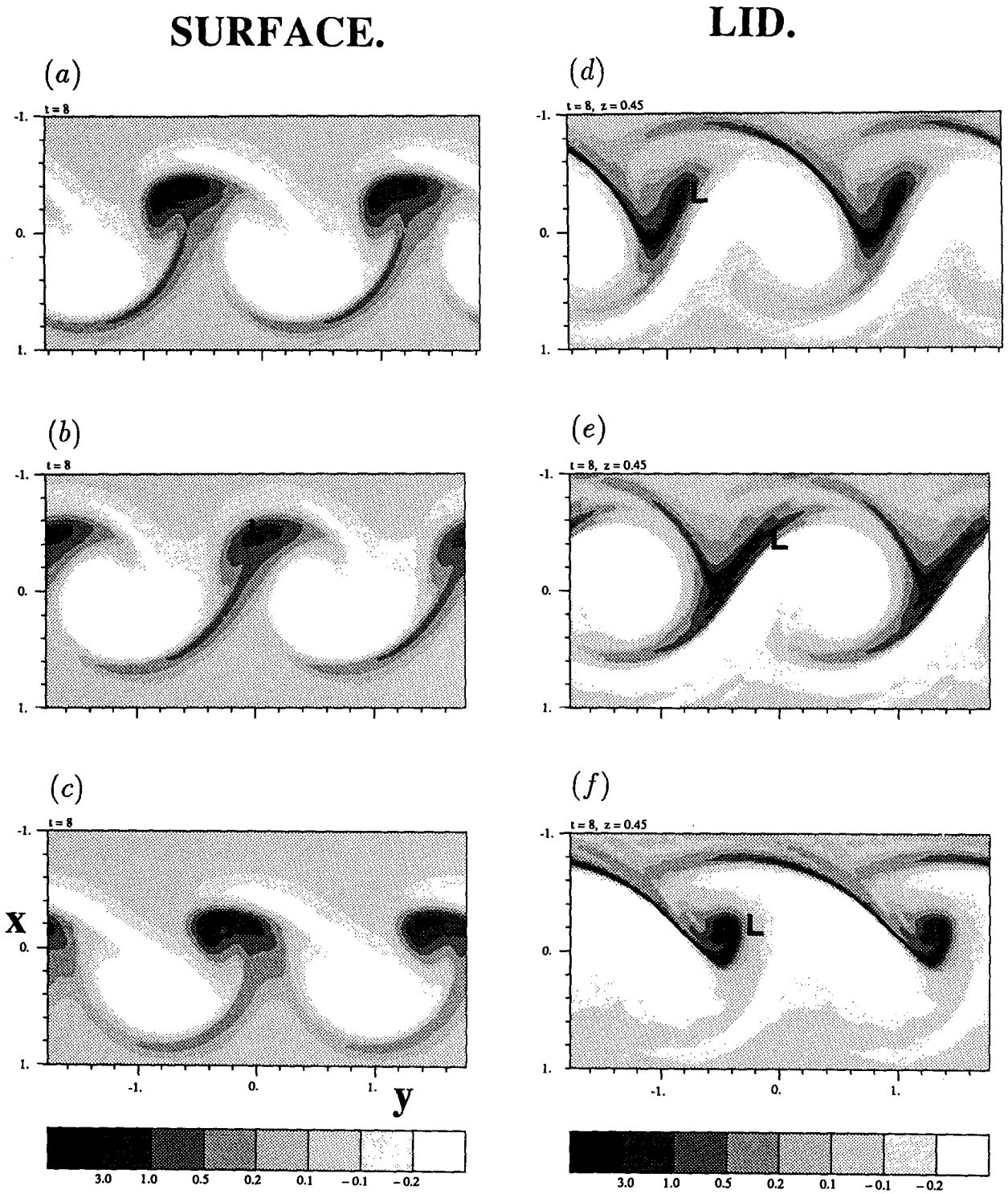

FIG. 10. Relative vorticity patterns of the nonlinear normal modes at time $t = 8$ (~day 4) displayed in physical space. The surface (panels a–c) and the upper-level (panels d–f) structures are shown for all the three cases with panels (a, d) corresponding to the no shear case, (b, e) to the anticyclonic shear case and (c, f) to the cyclonic shear case. The vorticity has been scaled in units of the Coriolis parameter, f, with cyclonic regions darker and the anticyclonic regions brighter. "L" denotes the position of the surface low pressure center.

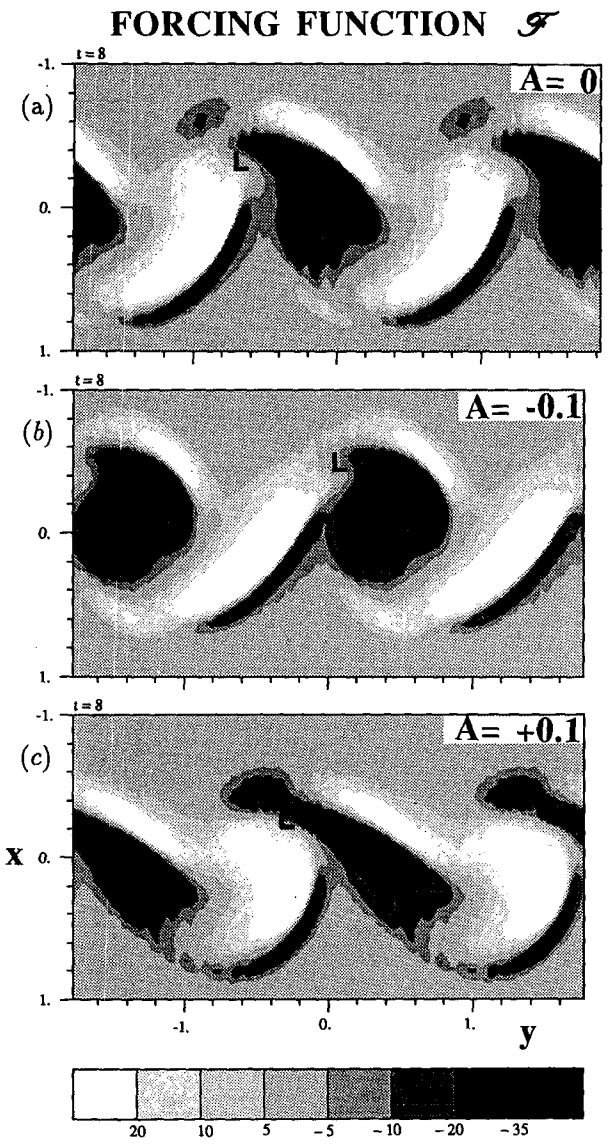

FIG. 11. The surface structure of the quasi-geostrophic forcing-function $\mathcal{F}$ at time $t = 8$ (~day 4) displayed in physical space for (a) the unsheared, (b) the anticyclonic shear and (c) the cyclonic shear cases. In the darker regions ($\mathcal{F} < 0$) the tendency is for positive vertical motion. Again L denotes the position of the surface low pressure center.

At around $t = 7$ there is a saturation event characterized by the complete removal of the surface zonal-mean baroclinicity in midstream, and the spanning of the original baroclinic zone ($-0.4 < x < 0.4$) by the lateral displacement of the midstream surface isentrope (cf. Held and Hoskins 1985). Thereafter the perturbations extend laterally beyond the domain of the original main baroclinic zone, and the zonal-mean surface baroclinicity reverses in midstream with a concomitant substantial enhancement of the thermal gradients on the lateral fringes. During this phase the modal structures of the perturbations develop finer scaled structures. At the ground the perturbations assume a distinct embryo form such that the "skull" (S) and "visor" (V) of these features are located astride the thermal extrema of the zonal mean field. Ambient positive (negative) shear enhances only the thermally positive (negative) embryos.

b. *The linkage between the mean flow and the cyclone tracks*

The lateral drift and relative zonal movement of the pressure systems displayed in Figs. 7–9 occur within, and are subject to, substantial changes in the zonal-mean pressure. Yet, as noted earlier, the thermal (and pressure) perturbations translate with approximately the phase speed of the linear normal modes—a result attributable to the compensating effect of the changes in the zonal-mean baroclinicity and zonal flow upon the phase propagation. This suggests that it is the north–south asymmetry of the pressure pattern accompanying the changes in the $\bar{V}$-field that determines the meridional displacement and the lateral scale of the simulated cyclones and anticyclones.

The development of the zonal mean flow ($\bar{V}$) on the bounding surfaces is shown in Fig. 15. During the development of the unsheared case a surface westerly jet (~15 m s^{-1}) is established in midstream with flanking but narrower easterly jets of comparable magnitude, while the amplitude of the upper level jet diminishes to almost the same value. For the sheared case the north–south asymmetry of the modes contributes, as anticipated earlier, to an enhancement of the ambient shear. In the $A = 0.1$ case the strength of this lateral shear at the ground is magnified by almost an order of magnitude in the $|x| \leq 0.5$ region. This sustains a westerly jet (~25 m s^{-1}) on the southern fringe of this region and a comparable easterly jet on the northern fringe. At the lid the jet is displaced southwards without loss of amplitude and again a domain of substantial positive shear is established across the entire $|x| \leq 0.5$ region.

These changes in the $\bar{V}$-field (and the related modifications of the zonal-mean pressure field) are linked to the track of the pressure extrema—the lateral movement of the surface highs and lows corresponds well at least up to the time of saturation with the lateral movement of the extrema in the zonal-mean pressure field (compare Figs. 7–9 and 15). Likewise the relative zonal movement of the northern and southern extremities of the thermal perturbations (and hence of the highs and lows) is linked to the modifications of the zonal-mean flow.

Note in passing that the changes in the $\bar{V}$-field are themselves interpretable in terms of the $\bar{\theta}$ field. For example, at the initial instant the $\bar{\theta}$ field at the ground (top) is associated with an in situ easterly (westerly) jet, and the subsequent reduction of the midstream baroclinicity at both levels implies a reduction in the strength of these "virtual" jets.

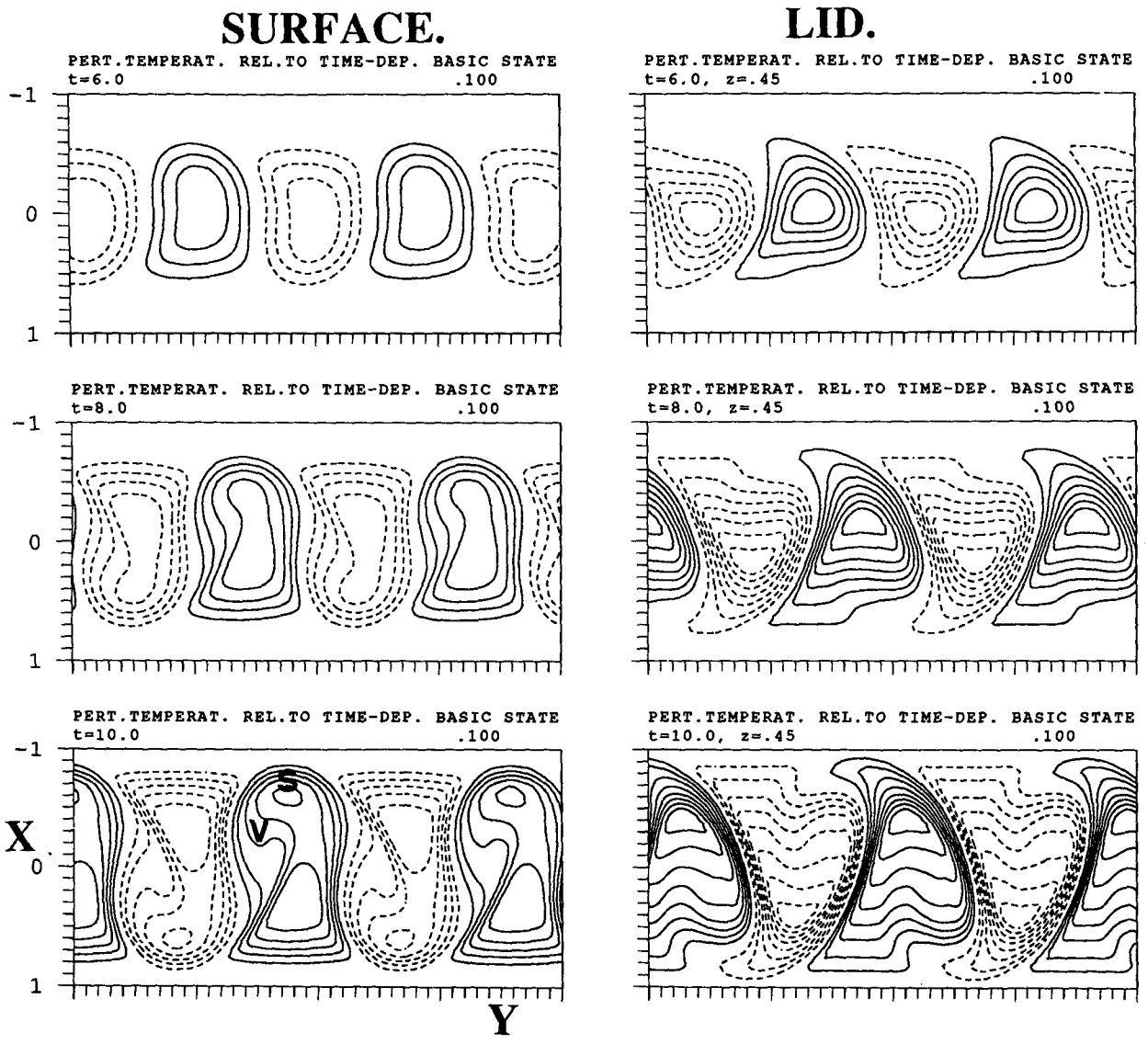

FIG. 12. Time sequence in geostrophic space of the potential temperature deviation away from the zonal-mean for the unsheared case at times t = 6, 8 and 10 (~day 3, 4 and 5). Surface fields are shown on the left and the upper-level fields on the right. The isoline spacing is 0.1 (~1.4 K); and negative contours are dashed. (The symbols S and V are identified in the text.)

c. *Frontal dynamics*

Frontal development is often viewed in terms of the establishment of a localized elongated broad band of baroclinicity by the larger-scale flow with the frontogenesis following in response to the activity of the ambient shear/deformation field. In all three of the present cases the initial wave development provides, respectively, ahead, and to the southwest, of the growing cyclone a suitable setting for warm and cold fronts. However, the difference in relative movement of the pressure systems significantly alters the strength of the ambient deformation field in these two frontogenetic regions. From a dynamical standpoint it is the combination of the thermal and wind fields, as defined by the quasi-geostrophic forcing function ($\mathcal{F}$), that directly forces the vertical motion and hence the vorticity generation in the frontal region.

Figures 10 and 11 display the surface distribution of the $\mathcal{F}$ field and the relative vorticity field at t = 10 for all three cases. Comparison of these figures indicates that despite the comparable strength of the forcing in the cold frontal region there is a marked difference in the in situ vorticity generated in the $A = \pm 0.1$ cases. Likewise, for the positive shear case there is no evidence of an elongated vorticity band linked to the warm front despite the significant forcing in that region. These are not inconsistent features since it is not the local strength

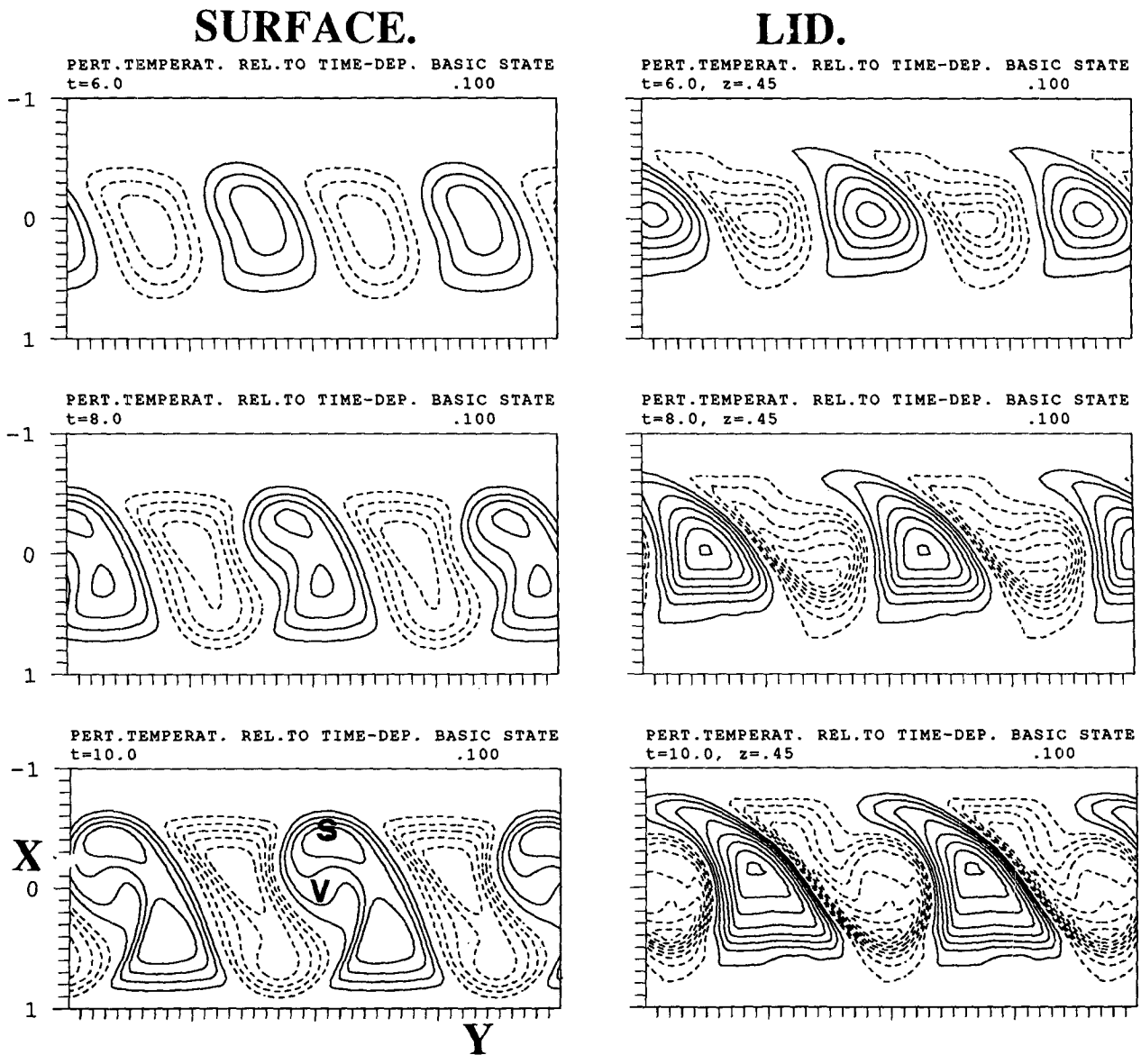

FIG. 13. As Fig. 14 but for the case of cyclonic shear ($A = +0.1$).

of the $\mathcal{F}$ forcing that determines the net change in the vorticity of a fluid element but rather the Lagrangian time history of the forcing experienced by the individual fluid elements. An inference is that there is a marked difference in the strength of relative flow of fluid elements through the elongated cold and warm frontal bands of $\mathcal{F}$ forcing. This in turn suggests a dynamical distinction between the cold and warm fronts. Consideration of the PV dynamics indicates that the surface and upper-level thermal patterns are linked in the case of a cold front to surface-level frontal flow directed, respectively, away from and toward a cyclone, while the opposite prevails for a warm front. Rigorous substantiation of the distinction would, however, require detailed kinematic analysis and is not pursued here.

d. Single level and interlevel interactions

The finer scale features of the surface thermal perturbations fields (θ') can be identified directly with distinct features of the front–cyclone palette:

- the northerly located visor (**V**) and skull (**S**) within the warm surface thermal anomaly together demark the central warm core/seclusion and the bent-back portion of the warm front;
- the interface of the NE portion of a warm anomaly with the neighboring northwest portion of the cold

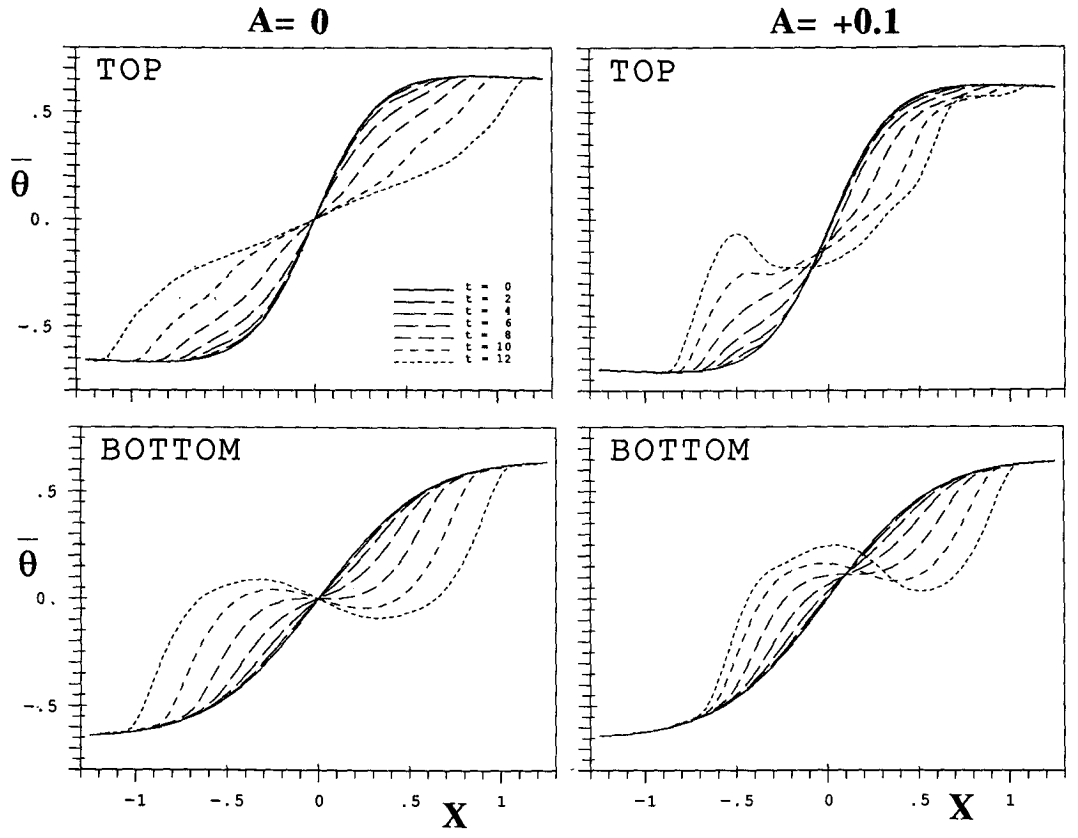

FIG. 14. Meridional profiles of the zonally averaged potential temperature field $\bar{\theta}(X)$ at both bounding surfaces for the unsheared case (on the left) and the cyclonic shear case (on the right). The scaling is in accord with Table 1.

anomaly represents the θ' signature of the warm front, and likewise the interface of the warm southwest portion and cold southeast portion is the cold frontal region;

- the visor-to-throat region of the warm anomaly corresponds to the location of the frontal fracture.

Similar linkages can be made between the θ' pattern and the salient flow features at the upper level, for example, the frontal structures and the incipient thermal cutoffs.

Here we consider the dynamical origin of the foregoing features by examining the linkage of the θ' and v' fields. Recall that from a PV standpoint the thermal perturbations on the bounding surfaces determine, for our system, the entire flow field including that on the bounding surfaces. Thus, the perturbation field, $\theta' = \psi'_Z$, on one bounding surface is associated with a perturbation flow-field response on both bounding surfaces. These single-level and interlevel effects are defined by the following decomposition of the perturbation streamfunction field:

Let:

$$\psi' = \psi'_0 + \psi'_T,$$

where

$$\nabla^2\psi'_0 = 0 \quad \text{with} \quad \psi'_Z = \begin{cases} \theta'_0 & \text{on} \quad Z = 0 \\ 0 & \text{on} \quad Z = Z_T, \end{cases}$$

and

$$\nabla^2\psi'_T = 0 \quad \text{with} \quad \psi'_Z = \begin{cases} 0 & \text{on} \quad Z = 0 \\ \theta'_T & \text{on} \quad Z = Z_T. \end{cases}$$

Thus (ψ'_0, ψ'_T) define the contributions to the flow response at a given time that can be attributed directly to, respectively, the perturbation potential temperature fields at the surface and the lid. An example of the resulting partitioned flow fields at the surface is shown in Fig. 16 for one particular time ($t = 10$). A clear appreciation of the relative contributions of the in situ and far-field effects can be derived by inspecting the time sequence of such flows and overlaying them with the related θ'-field. For example, the regions of substantial surface deformation in the in situ and far-field patterns directly influence the contribution to surface frontogenesis. Such considerations indicate that interlevel effects serve primarily to increase the amplitude of the isentropic displacements before, during, and after

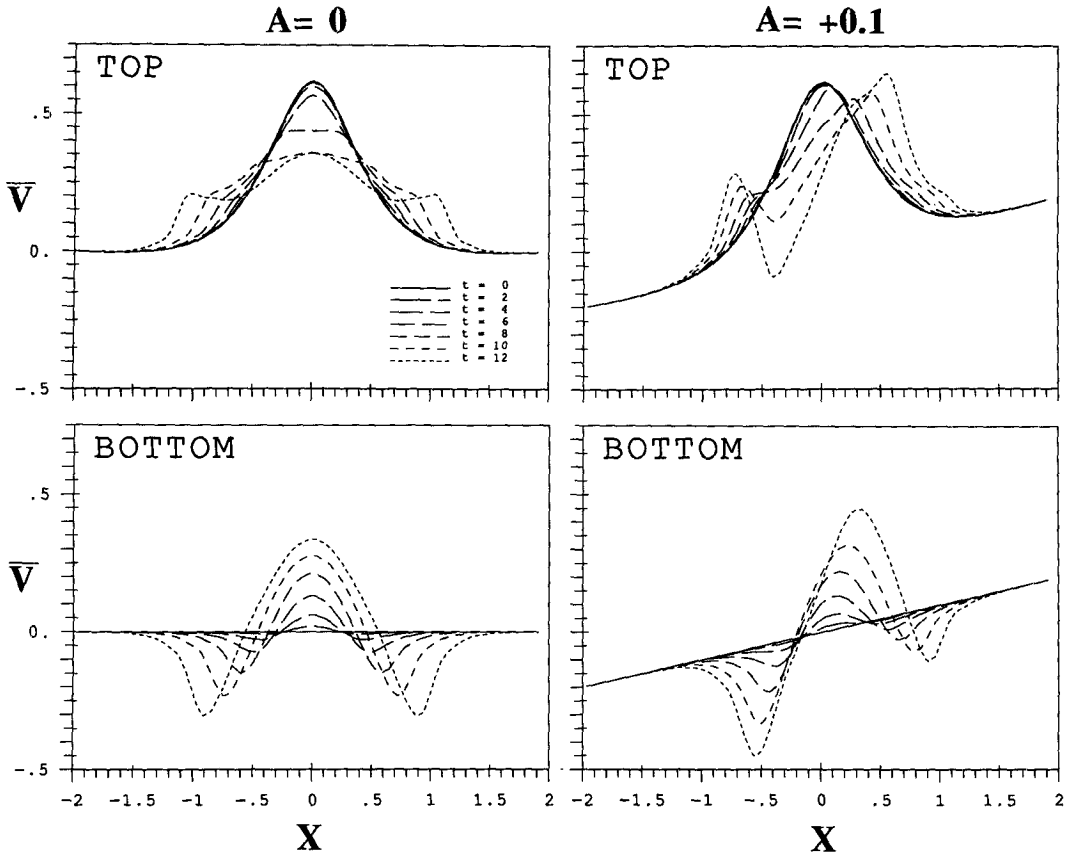

FIG. 15. As Fig. 14 but for the zonally averaged zonal wind speed $\bar{v}(X)$.

saturation. Thus they generate and accentuate the northernmost portion of the surface warm front (i.e., the skull) and the lateral extension of the upper-level trough–ridge features (see Figs. 7–9). Single-level induced flow components act frontogenetically upon the linear portions of the upper- and lower-level fronts. Both single and interlevel effects prove to be important in initiating the warm air seclusion, the fracture of the cold front and the upper-level cutoff features.

Once established, the northern portion of the warm front (the skull) and the seclusion (the visor) can mutually enhance one another across the extremum in the zonal-mean $\bar{\theta}$ field. Indeed, the coexistence of such a thermal extremum together with a colocated reversal in sign of the mean zonal flow constitutes conditions that can sustain a rapid normal-mode instability (Schär and Davies 1990). The physics, but not the origin, of the mutual reinforcement in the present case is the same as that for the instability.

In the presence of ambient barotropic shear the initial horizontal tilt of the mode away from the meridian is increased by the rapid quasi-linear enhancement of the barotropic shear. In terms of the relative phase of the perturbations in the vertical, a positive shear induces an initial northward (southward) shift of the upper (lower) level features, and this is amplified in the post-saturation phase. Hence the influence of the upper-level thermal pattern upon the surface wind field is stronger in the north and the finer scale features of the positive (negative) surface thermal anomalies are enhanced (suppressed).

The nature of the tilt and the warm–cold asymmetry of the thermal anomalies in the $A > 0$ case account, for example, for the strengthening of the warm front and the stronger dislocation of the cold front. The relative contributions of the surface and upper-level thermal anomalies to the *surface* flow field in the frontal regions also relate to the aforementioned dynamical distinction between cold and warm fronts. As noted earlier the two contributions tend to counter one another, but in the presence of shear there is a strong modification of their relative amplitude.

6. Some further considerations

a. Relationship to observed features

The simulated concurrent development of cold and warm fronts, the occurrence of frontal fracture, incipient seclusion, and a bent-back warm front arching across the inner northern core of the cyclone are surface

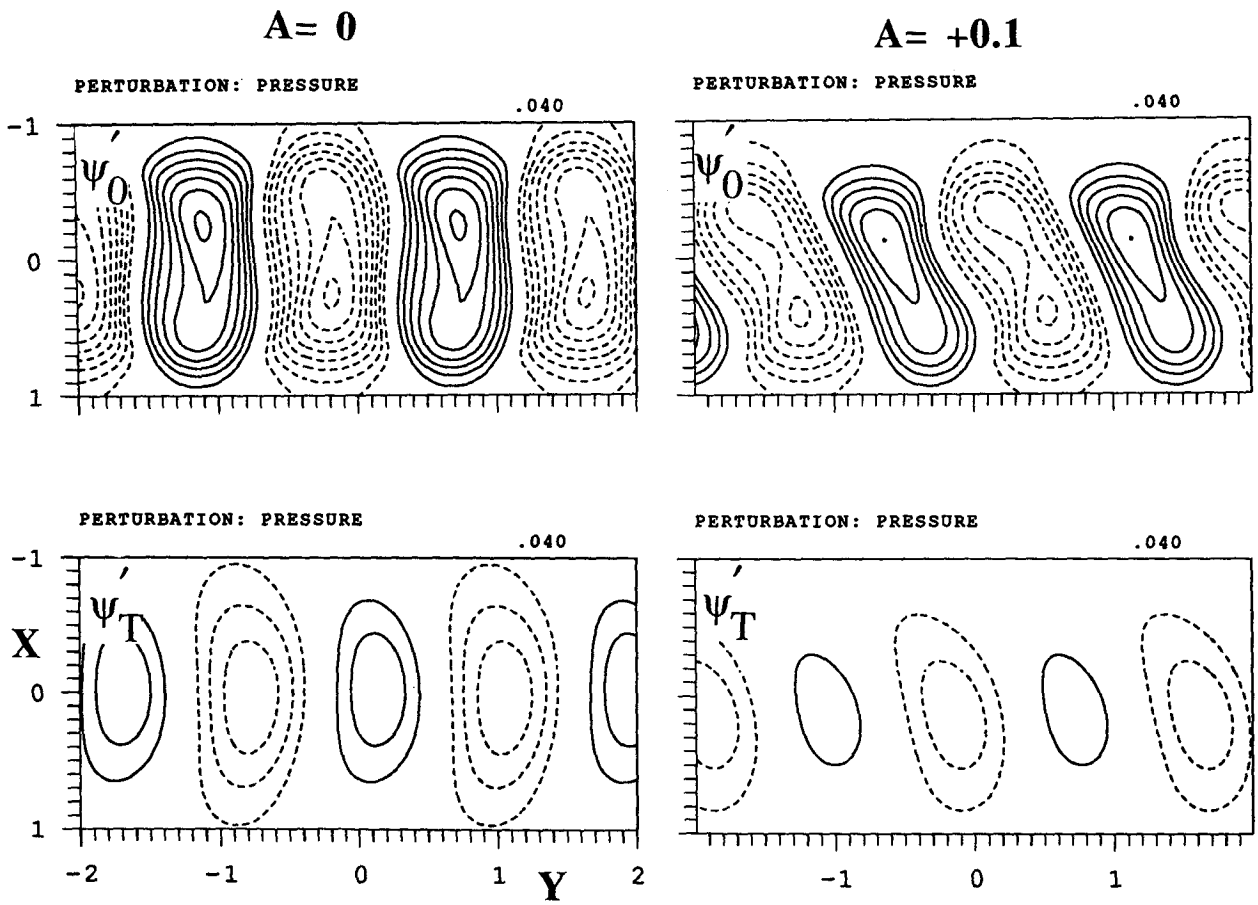

FIG. 16. A display of the "in situ" and "far-field" effects of the perturbation potential temperature fields shown in geostrophic space and valid at the surface for the time $t = 10$ (~day 5). The top panels show the in situ–induced component, ψ'_0, and the bottom panels show far-field–induced component), ψ'_T. The unsheared case is on the left and the cyclonic shear case on the right. (The isoline spacing is 0.04, ~4 hPa, and negative contours are dashed.)

features that replicate those detailed in recent observational studies (e.g., see Shapiro and Keyser 1990). The large variation in the simulated frontal patterns with cyclones evolving in tandem with a cold front and with (or without) an attendant warm front is also within the observed spectrum.

At the upper-lid the simulation of realistic incipient cutoff cold (warm) air pools in positive (negative) shear relates closely to two main signatures detected in the tropospheric–stratospheric PV structure (Hoskins et al. 1985). The cold pools are the equivalent in the present model to an upper-level positive PV cutoff, and cutoffs are potential precursors of surface cyclogenesis (Bleck and Mattocks 1984; Hoskins et al. 1985). Again the (possibly ageostrophic) propagation of a jet streak through the trough in the upper-level flow (e.g., see Shapiro 1983) is a significant subsynoptic flow feature. There is no evidence of such an effect in these simulations. However, the location of the jet does shift from the rear to the fore of the trough with a change in sign of the initial barotropic shear.

A pertinent study from a more climatological standpoint is that of Wallace et al. (1988). They examined the variance of the high-pass filtered geopotential field of the midlatitude baroclinic waveguide to ascertain the location of storm tracks. The present results regarding the essentially zonal translation of the *perturbation* positive and negative thermal (and pressure) fields up to saturation time is in line with their conclusions (and with their interpretation of the simulations reported in HW). A caveat is that the disturbances within an atmospheric baroclinic waveguide are in effect traversing through and out of that region, whereas in our normal-mode setup the growing baroclinic wave induces an in situ reduction of the basic state baroclinicity and a reinforcement of the ambient barotropic shear.

Observational verification of the model-detected dependence of the latitudinal location and constitution of the front–cyclone palette upon the asymmetry within the ambient baroclinic zone is not straightforward. One recent study of the month-to-month variability of the

wintertime storm tracks/baroclinic waveguide revealed (Lau 1988, pp. 2724–2725) that northward and southward migration of these bands was accompanied by time-mean conditions associated, respectively, with negative and positive horizontal shear of the ambient zonal wind—a result in harmony with that of the present study.

b. *Limitations of the study*

The simplicity of the model and the approach adopted in this study place constraints upon the generality of the results.

1) SOME PHYSICAL IDEALIZATIONS

There are clearly stark limitations associated with the neglect of frictional and diabatic effects. These play a key role in some cyclogenesis events (e.g., see Uccelini 1990). In contrast, the present study illustrates the rich range of realistic flow structures that can be engendered by adiabatic processes in response to a *minor modification* of a purely uniform PV atmosphere. An inference is that the ingredients of the front–cyclone palette can, in principle, be established by adiabatic dynamics and then enhanced/modified by diabatic effects. The results also provide a yardstick with which to assess or compare the modifications thought to be attributable to other (often highly parameterized) effects.

Again the sensitivity of the flow response to a break in the symmetry of the fluid system was demonstrated in the present study by introducing only *a uniform barotropic shear* component to the basic state. However, additional simulations indicate that the presence of *a latitudinally and vertically confined band of lateral shear,* associated with a small asymmetry in the basic-state thermal distribution on a bounding surface, produces a similar response. Likewise, a symmetric jet subjected to a broad but confined finite-amplitude asymmetric initial thermal disturbance at the surface (with a resulting lateral shear of the ambient environment) exhibits comparable sensitivity (Schär 1989). Such results are indicative of the influence of shallow near-surface, or tropopause-level, internal potential vorticity distributions, and of the potentially significant effects of other modulated initial conditions upon the later phase of the development. Thus, these simulations suggest that the flow sensitivity reported earlier for one particular idealized setting has a more general validity.

2) SEMIGEOSTROPHY

The semigeostrophic system has provided a fruitful and attractive conceptual framework for heuristic studies of the synoptic/subsynoptic dynamics. It also has certain desirable mathematical properties not possessed by the PE set, for example, for the representation of discontinuous flows (Cullen and Shutts 1988). Again, its accuracy in representing two-dimensional frontogenesis is often notable (e.g., see Davies and Müller 1988). However, formal scale analysis (McWilliams and Gent 1980) and studies of certain special flows (Allen et al. 1990) suggest that in three dimensions its quantitative accuracy will be significantly reduced.

Thus, one issue is the validity of the semigeostrophic set of equations as an appropriate limit-form of the primitive equations for the simulation of the front–cyclone palette. Several studies of baroclinic wave growth have been undertaken with high resolution PE and/or balanced flow models (Mudrick 1974; Simmons and Hoskins 1976; Gall 1977; Hoskins 1983; Takayabu 1986; Polavarapu and Peltier 1990; Snyder et al. 1991). The results indicate that, for the same (or almost the same) baroclinic jetlike basic state, the linear PE normal modes in comparison with the balanced modes exhibit in the vertical a greater tilt to the north, and in the horizontal a greater tilt and phase change of the northerly wing relative to the southerly wing. The modes can also possess markedly different distributions of the horizontal eddy momentum flux. In the nonlinear development the PE modes display a predilection to develop deeper and more vertically coherent lows, weaker and more strongly tilting highs, bent-back warm fronts, and pronounced seclusions.

Thus, unless the particular basic states for which the simulations were undertaken are in some sense atypical, these differences are indicative of the possible inappropriateness of simulating baroclinic growth with the semigeostrophic equations.

In this respect we note that the results of the present study show that:

- the symmetry state of the semigeostrophic system is in essence a bifurcation point with the structure of the nonlinear development differing radically in response to the sign of the asymmetry,
- the features that distinguish the PE simulations are akin to those of a semigeostrophic simulation with a weak positive shear. For example, the PE results obtained by Snyder et al. (1991) resemble and are comparable with semigeostrophic simulations undertaken with a lateral shear of approximately only $10^{-2} f$.

Thus, if a similar bifurcation exists for the PE system but with a slight "shift" of the bifurcation point in parameter space then the aforementioned differences between the two types of simulations might be linked to this dynamical effect.

To pursue this hypothesis further, consider the equation for the time rate of change of the "zonally" and vertically averaged momentum for the full primitive equation system of an incompressible fluid located between two flat plates on an f plane; i.e.,

$$\frac{\partial \bar{v}}{\partial t} = -\frac{\partial}{\partial x}[\overline{uv}].$$

Now the overbar denotes the double spatial-averaging procedure. On introducing a decomposition of the flow into geostrophic (subscript g) and ageostrophic (subscript a) components, the equation can be rewritten successively as

$$\frac{\partial \bar{v}}{\partial t} = -\frac{\partial}{\partial x}[\overline{u_g v_g} + \overline{u_a v_g} + \overline{u_g v_a} + \overline{u_a v_a}],$$

$$= -\frac{\partial}{\partial x}\left[\underbrace{\overline{u_g v_g}}_{\text{I}} - \underbrace{\frac{1}{f}\left\langle \overline{v\frac{Dv}{Dt}}\right\rangle}_{\text{IIa}} - \underbrace{\left\langle \overline{u\frac{Du}{Dt}}\right\rangle}_{\text{IIb}} + \underbrace{\frac{1}{f^2}\overline{\frac{Du}{Dt}}\,\overline{\frac{Dv}{Dt}}}_{\text{III}}\right].$$

The fluxes I, II, and III are, respectively, of O (1), O (R_0), and O (R_0^2) where $R_0 = (f\tau)^{-1}$, and τ is a Lagrangian time scale for the advection. To O (R_0) a reasonable approximation of the tendency is given by

$$\frac{\partial \bar{v}}{\partial t} \approx -\frac{\partial}{\partial x}\left[\underbrace{\overline{u_g v_g}}_{\text{I}} + \underbrace{\frac{1}{2f}\left\langle -\overline{\frac{\partial v_g^2}{\partial t}} + \overline{\frac{\partial u_g^2}{\partial t}}\right\rangle}_{\text{IIa}\quad\text{IIb}}\right].$$

The first component of the flux (term I) is the usual expression for the quasi-geostrophic momentum flux. Term IIa is induced by the ageostrophic advection of momentum and a contribution of this form is included in the semigeostrophic system. Term IIb [cf. Stone 1972; Eq. (3.19a)] involves the geostrophic advection of ageostrophic momentum and is neglected in the semigeostrophic formulation. Moreover, for a *growing* baroclinic wave with the maximum perturbation somewhere in midstream this latter term induces a southward flux of momentum and a positive barotropic shear of the zonal mean flow. Thus, in comparison with a semigeostrophic system the PE system includes an additional O (R_0) effect that, for growing waves, induces an asymmetric response associated with the generation of lateral barotropic shear. This effect is consistent with the foregoing hypothesis. In a flow state that is "almost symmetric" the presence of this flux convergence, although small, might be crucial; once the lateral shear is established it could be amplified by first-order geostrophic effects. In a noncritical configuration the prevailing asymmetry could dominate the development.

It is, however, important to note that the difference between the vertically averaged momentum fluxes of PE and semigeostrophic simulations of the same flow state need not be linked exclusively to term IIb since the PE system could also generate a different geostrophic contribution. The aforementioned comparison studies provide evidence of such an effect.

In view of the foregoing, it would be useful to undertake further comparisons of PE and semigeostrophic simulations of baroclinic wave growth for highly asymmetric basic states (of both signs) and/or finite amplitude initial perturbations.

7. Final remarks

It has been demonstrated that an ambient barotropic shear superimposed upon a baroclinic jetlike flow exerts a substantial influence upon the palette of fronts and cyclones that appear in the finite-amplitude regime of a semigeostrophic normal-mode wave development. The presence of the shear modifies:

- the track, strength, horizontal scale, shape and the vertical tilt of the highs and lows;
- the occurrence, intensity, and vertical coherence of the fronts.

This variation of the front–cyclone palette has been shown to be intrinsically related in the linear phase to the shear-induced displacement of the normal mode's critical-surface relative to the main baroclinic zone, and in the nonlinear phase to single-level and interlevel effects.

Specific features of the palette shed light upon some of the enigmas noted in the Introduction. For example,

- the fracture of the cold front compared with the nonoccurrence of the classic occlusion process,
- the predominantly ageostrophic as opposed to the geostrophic signal of the simulated warm front compared with the amorphous nature of observed warm frontal structures,
- the sensitivity of the palette to asymmetries compared with the reasonable cold and warm frontal forecasts of NWP models operating presumably with the appropriate atmospheric asymmetries.

In the previous section attention was drawn to the differences between PE and semigeostrophic simulations of baroclinic wave growth. Here we seek to stress that the differences between semigeostrophic simulations undertaken with uniform positive and negative values for the ambient lateral shear are appreciable. For example, the difference in the pressure pattern between the $A = (-0.1$ and $+0.1)$ cases is, at $t = 10$, equivalent to an 800 km meridional shift of the low, a 50% change in the high-to-low separation, a 50% change in the strength of the geostrophic wind in the neighborhood of the cold front, an 18 hPa difference in the depth of the low, and a 50 m s^{-1} change in the zonal-mean wind on the fringe of the baroclinic zone. This range of variations spans a significant part of that

associated with observed cyclones and fronts, and is achieved by the mere inclusion of a zonally aligned pressure band with a gradient of ~2.5 hPa over 1000 km in the zonal-mean pressure field.

Acknowledgments. It is a pleasure to thank Chris Snyder and Craig Bishop for stimulating comments on the differences between the primitive equation and the semigeostrophic simulations of baroclinic waves.

APPENDIX

On a Symmetry Property of Semigeostrophic Normal Modes

Here we adopt the notation introduced in section 2 and outline the basis for the following theorem:

Any two-dimensional basic state that is symmetric in transformed space gives rise to normal modes that possess, in both their linear and finite-amplitude phase, the following symmetry property,

$$\Psi(X, Y, Z, T) = -\Psi(-X, Y - \lambda/2, Z, T), \quad \text{(A1)}$$

where λ denotes the wavelength of the mode,

Similar relations pertain for the potential temperature and relative vorticity and likewise the geostrophic flow components satisfy the equations,

$$u_g(X, Y, Z, T) = -u_g(-X, Y - \lambda/2, Z, T), \quad \text{(A2a)}$$

$$v_g(X, Y, Z, T) = +v_g(-X, Y - \lambda/2, Z, T). \quad \text{(A2b)}$$

To prove this result, note that

- a symmetric basic state [e.g., Eq. (2.4) with $A = 0$] automatically fulfills the condition (A1); and
- both the normal mode and the associated twin mode obtained by reflection about the Y axis satisfy the linearized thermodynamic equation (2.3b).

It follows that the normal modes occur either in symmetric degenerate pairs or are themselves symmetric about $X = 0$. On excluding the degenerate case, the periodicity in the Y direction allows the modes to satisfy (A1). Furthermore, the temperature tendencies on the horizontal bounding surfaces ($Z = 0, Z_T$) can sustain the same symmetry since

$$\frac{\partial}{\partial T}\theta(-X, Y - \lambda/2) = -[-u_g(X, Y)]\frac{\partial}{\partial X}\theta(X, Y)$$

$$- v_g(X, Y)\left[-\frac{\partial}{\partial Y}\theta(X, Y)\right] = -\frac{\partial}{\partial T}\theta(X, Y).$$

Hence, in association with the elliptic equation (2.2), this property is also true for the potential temperature tendency in the entire flow domain.

REFERENCES

Allen, J. S., J. A. Barth and P. A. Newberger, 1990: On intermediate models for barotropic continental shelf and slope flow fields. Part I: Formulation and comparison of exact solutions. *J. Phys. Oceanogr.*, **20,** 1949–1973.

Bleck, R., and C. Mattocks, 1984: A preliminary analysis of the role of potential vorticity in alpine lee cyclogenesis. *Contrib. Atmos. Phys.*, **57,** 357–368.

Browning, K. A., 1990: Organization of clouds and precipitation in extratropical cyclones. *Extratropical Cyclones: The Erik Palmen Memorial Volume,* Amer. Meteor. Soc., 265 pp.

Cullen, M. J. P., and G. J. Shutts, 1988: Numerical modeling of balanced atmospheric flow. *Comput. Math. Appl.*, **16,** 69–71.

Davies, H. C., and J. C. Müller, 1988: Detailed description of deformation-induced semigeostrophic frontogenesis. *Quart. J. Roy. Meteor. Soc.*, **114,** 1201–1219.

Gall, R., 1977: Some non–quasi-geostrophic effects in linear baroclinic waves. *J. Atmos. Sci.*, **105,** 1039–1051.

Held, I. M., and B. J. Hoskins, 1985: Large-scale eddies and the general circulation of the troposphere. *Adv. Geophys.*, **28,** 3–31.

Hoskins, B. J., 1975: The geostrophic momentum approximation and the semigeostrophic equations. *J. Atmos. Sci.*, **32,** 233–242.

——, 1983: Dynamical processes in the atmosphere and the use of models. *Quart. J. Roy. Meteor. Soc.*, **109,** 1–22.

——, and N. V. West, 1979: Baroclinic waves and frontogenesis. Part II: Uniform potential vorticity jet flows. *J. Atmos. Sci.*, **36,** 1663–1680.

——, I. Draghici and H. C. Davies, 1978: A new look at the ω-equation. *Quart. J. Roy. Meteor. Soc.*, **104,** 31–38.

——, M. E. McIntyre and A. W. Robertson, 1985: On the use and significance of isentropic potential vorticity maps. *Quart. J. Roy. Meteor. Soc.*, **111,** 877–946.

Ioannou, P., and R. S. Lindzen, 1986: Baroclinic instability in the presence of barotropic jets. *J. Atmos. Sci.*, **43,** 2999–3014.

James, I. N., 1987: Suppression of baroclinic instability in horizontally sheared flows. *J. Atmos. Sci.*, **44,** 3710–3720.

Keyser, D., and M. J. Pecnick, 1987: The effect of along-front temperature variation in a two-dimensional primitive equation model of surface frontogenesis. *J. Atmos. Sci.*, **44,** 577–604.

Kleinschmidt, E., 1950: Über Aufbau und Entstehung von Zyklonen. *Meteor. Rundsch.*, **3,** 1–6.

Lau, N-C., 1988: Variability of the observed midlatitude storm tracks in relation to low-frequency changes in the circulation pattern. *J. Atmos. Sci.*, **45,** 2718–2743.

McWilliams, J. C., and P. R. Gent, 1980: Intermediate models of planetary circulations in the atmosphere and ocean. *J. Atmos. Sci.*, **37,** 1657–1678.

Moore, G. W. K., and W. R. Peltier, 1989: Nonseparable baroclinic instability. Part I: Quasi-geostrophic dynamics. *J. Atmos. Sci.*, **46,** 57–78.

Mudrick, S. E., 1974: A numerical study of frontogenesis. *J. Atmos. Sci.*, **31,** 869–892.

Newton, C. W., and E. O. Holopainen, 1990: *Extratropical Cyclones: The Erik Palmen Memorial Volume.* Amer. Meteor. Soc., 265 pp.

Palmen, E., 1951: The aerology of extratropical disturbances. *Compendium of Meteorology,* T. F. Malone, Ed., Amer. Meteor. Soc., 559–620.

Polavarapu, S. M., and W. R. Peltier, 1990: The structure and nonlinear evolution of synoptic scale cyclones: life cycle simulations with a cloud scale model. *J. Atmos. Sci.*, **47,** 2645–2672.

Reed, R. J., 1990: Advances in the knowledge and understanding of extratropical cyclones during the past quarter century: an Overview. *Extratropical Cyclones: The Erik Palmen Memorial Volume,* Amer. Meteor. Soc., 265 pp.

Schär, C., 1989: Dynamische Aspekte der aussertropischen Zyklogenese. Theorie und numerischen Simulation im Limit der balancierten Strömungssysteme. Dissertation E.T.H. Zürich, 241 pp.

——, and H. C. Davies, 1990: An instability of mature cold fronts. *J. Atmos. Sci.*, **47,** 929–950.

Shapiro, M. A., 1983: Mesoscale weather systems of the central United States. The National STORM Program: Scientific and Technological Bases and Major Objectives, R. A. Anthes, Ed., 3.1–3.77 [Available from NCAR, P.O. Box 3000, Boulder CO 80307]

——, and D. Keyser, 1990: On the structure and dynamics of fronts, jet streams, and the tropopause. *Extratropical Cyclones: The Erik Palmen Memorial Volume,* Amer. Meteor. Soc., 265 pp.

Simmons, A. J., and B. J. Hoskins, 1976: Baroclinic instability on the sphere: normal modes of the primitive and quasi-geostrophic equations. J. Atmos. Sci., **33,** 1454–1477.

——, ——, 1980: Barotropic influences on the growth and decay of nonlinear baroclinic waves. *J. Atmos. Sci.*, **37,** 1679–1684.

Snyder, C., C. Skamarock and R. Rotunno, 1991: A comparison of primitive-equation and semigeostrophic simulations of baroclinic waves. *J. Atmos. Sci.*, in press.

Stone, P. H., 1972: On nongeostrophic baroclinic stability. Part III: The momentum and heat transports. *J. Atmos. Sci.*, **29,** 419–426.

Takayabu, I., 1986: Roles of the horizontal advection on the formation of surface fronts and on occlusion of a cyclone developing in the baroclinic westerly jet. *J. Meteor. Soc. Jpn.*, **64,** 329–345.

Thorncroft, C., and B. J. Hoskins, 1990: Frontal cyclogenesis. *J. Atmos. Sci.*, **47,** 2317–2336.

Uccellini, L., 1990: Processes contributing to the rapid development of extratropical cyclones. *Extratropical Cyclones: The Erik Palmen Memorial Volume,* Amer. Meteor. Soc., 265 pp.

Valdes, P. J., and B. J. Hoskins, 1988: Baroclinic instability of a zonally averaged flow. *J. Atmos. Sci.*, **45,** 1584–1593.

Wallace, J. M., and P. V. Hobbs, 1977: *Atmospheric Science. An Introductory Survey.* Academic Press, 467 pp.

——, G-H. Lim and M. L. Blackmon, 1988: Relationship between cyclone tracks, anticyclone tracks, and baroclinic waveguides. *J. Atmos. Sci.*, **45,** 439–462.

Woodroffe, A., 1984: Short-range weather forecasting—A current assessment. *Weather,* **39,** 298–310.